American Journal of Engineering and Applied Sciences

Research Article

On a Novel Closed-Form Analytical Solution for Unsteady Solidification: Theory and Application

Gueber Elias Mendes Santos Júnior, Fernando S. Rocha, Ana Beatriz S. Silva, Davi A. R. Carmo, Mateus O. Silva and Ivaldo L Ferreira

Faculty of Mechanical Engineering, Federal University of Pará, UFPA, Augusto Corrêa Avenue 1,66075-110, Belém, PA, Brazil

Article history
Received: 17-11-2025
Revised: 03-02-2026
Accepted: 23-03-2026

Corresponding Author:
Ivaldo L Ferreira
Faculty of Mechanical Engineering, Federal University of Pará, UFPA, Augusto Corrêa Avenue 1,66075-110, Belém, PA, Brazil
Email: ileao@ufpa.br

Abstract: Numerical modeling of transient solidification under convective boundary conditions presents a significant challenge because accurately tracking the solid–liquid interface is essential for obtaining a stable solution. Although analytical solutions are generally straightforward to apply, the growing demand for energy storage driven by mismatches between supply and demand in renewable-energy systems requires reliable predictive tools for Latent Heat Thermal Energy Storage (LHTES) applications. In this work, we compare a classical analytical solution for the transient solidification of pure and eutectic phase-change materials with a recently derived formulation that provides a complete treatment of the Biot number. The comparison is performed in the context of sizing LHTES reservoirs and selecting appropriate phase-change materials. The results demonstrate that the new formulation accurately predicts the velocity of the solid–liquid interface, the thermal gradient, and the cooling rate, offering improved reliability over the classical approach.

Keywords: Closed-Form Analytical Solution, Convective Boundary Condition, Solidification Kinetics, Latent-Heat Thermal Energy Storage (LHTES), Numerical Modeling, Experimental Validation

Introduction

Solid liquid phase transformations are fundamental to a wide range of scientific and technological fields. In geophysics, they control weather patterns, the water cycle, igneous rock formation, glacier dynamics, and ice sheet evolution; in materials science and engineering, they underpin metal casting, semiconductor fabrication, and cement production; and in chemistry and pharmaceuticals, they are central to crystallisation processes used for purification. On a macroscopic scale, these transformations are manifested as a moving interface that separates the solid and liquid phases. During melting, the liquid–solid interface advances into the material until the solid is completely consumed (Jost, 1952, Carslaw and Jaeger, 1959). The motion of this interface is governed by a heat balance condition: the latent heat released (or absorbed) per unit volume must be supplied (or removed) by the heat fluxes on the solid and liquid sides of the interface. Problems of this type constitute the classical Stefan problem, named after the Slovenian physicist Jožef Stefan, who first formulated this class of moving boundary problems (Furzeland, 1977). Classical analytical solutions for the one dimensional Stefan problem can be found in the literature (Crank, 1984).

In many practical solidification and melting processes, the temperature at the exposed surface (usually taken as x=0) is governed by a convective (Robin) boundary condition rather than by a prescribed temperature. Analytical solutions that incorporate such a convective condition for pure metals and eutectic alloys are comparatively scarce (Mori and Akari, 1976; Alexandrov et al., 2018; Crank, 1981; Furzeland, 1977; Hunziker, 2001; Rappaz et al., 2003; Voller, 2009; Fezi and Krane, 2015; Saha and Dutta, 2015; Tourret and Karma 2016; Monde and Chakraborty, 2017; Álvarez et al., 2018; Alexandrov et al 2018; Carvalho et al., 2021; Akhtar et al., 2021; Cassia et al., 2022; Garg and Singhal; 2022 Liet al., 2022; Alsulami et al., 2023). Clyne and Garcia presented an exact solution for a generalized solidification problem under the assumption of a constant interfacial heat transfer coefficient, using the Virtual Adjunct Method, which treats the interfacial resistance as a set of virtual solid or mould layers (Garcia and Prates, 1978). Building on this idea, Garcia and

coworkers derived analytical solutions for binary alloys (Garcia et al., 1979; Clyne and Garcia, 1980; Lipton et al.,1982; Quaresma et al., 2000). Davay obtained a solution for directional solidification that includes the motion of the casting at the interface by simultaneously solving the transient heat equations for the mould, the gas gap, the solid, the liquid, and any contaminating layers (Davey, 1993).

The accelerating threat of global warming, driven by anthropogenic greenhouse gas emissions (Yang et al., 2021), underscores the need for efficient renewable energy technologies. Latent Heat Thermal Energy Storage (LHTES) has emerged as a key enabling technology because Phase Change Materials (PCMs) can store and release large amounts of energy during solid–liquid transitions. Compared with sensible heat storage (SHTES), LHTES can store 5 14 times more heat per unit volume (Zhou and Wu, 2019; Pasupathy et al., 2008; Liu et al., 2023; Govindasamy and Kumar, 2023; Wang et al 2023). The authors applied a lumped capacitance (or "lumped") solution, which assumes that the solidified material (or PCM) behaves as a spatially uniform body so that internal temperature gradients can be neglected, an assumption that is valid when the Biot number $Bi = hL/k$ is much smaller than 1. Under this hypothesis, the energy balance reduces to an ordinary differential equation, $\rho V c_p \frac{dT}{dt} = hA\,(T_\infty - T)$, whose solution is the classic exponential decay $T(t) = T_\infty + (T_0 - T_\infty)\exp[-hA/(\rho V c_p)\,t]$.. For transient solidification the latent heat is incorporated by augmenting the effective heat capacity with the term $L\frac{d\alpha}{dt}$ (where α is the solid fraction), giving a piecewise solution:

(i) Sensible heat phases before and after melting, described by the exponential law above
(ii) An isothermal phase change interval at the melting temperature T_m in which the interface position evolves according to $\rho L \frac{dX}{dt} = hA\,(T_\infty - T_m)$

The resulting closed form expressions provide quick estimates of the solid liquid interface position, interface velocity, thermal gradient, and cooling rate, but they are accurate only for objects with low Bi and negligible internal conduction resistance. Accurate knowledge of PCM solidification and melting kinetics is therefore essential for sizing thermal reservoirs and for predicting system performance (Ivaldo et al., 2025).

Mendes Júnior has recently proposed a novel analytical framework for transient solidification, yielding four closed form solutions for pure and eutectic materials in one- and three-dimensional semi-infinite geometries. The approach explicitly incorporates convective surface conditions and melt superheat, and introduces a first order correction term that bridges the gap between second order and first order similarity solutions. This yields accurate predictions of thermal gradients, interface velocities, and cooling rates (Santos, 2024); a detailed derivation is given in Ivaldo et al. (2024). Nevertheless, the original formulation does not reproduce measured interface velocities satisfactorily, nor does it provide a means to evaluate the mean heat transfer coefficient. More recently, Trojan derived an exact solution for non-reactive unsteady heat conduction in a semi-infinite slab subject to a convective boundary condition, thereby extending the analytical toolbox for such problems (Trojan, 2014).

In the present work, we evaluate the thermal gradient, solid–liquid interface velocity, and cooling rate for a selection of metals and for water using:

(i) A classical analytical solution for solidification (Clyne and Garcia, 1980)
(ii) The recently introduced solution that fully resolves the Biot number (Santos, 2024)

The predictions are benchmarked against experimental measurements (Rocha et al., 2020; Marques et al., 2025) and against numerical simulations reported in the literature (Swaminathan and Voller, 1997; Ferreira et al., 2004). This comparative study highlights the strengths and limitations of each analytical approach and provides guidance for their use in the design of LHTES systems and in the modelling of natural solidification phenomena.

Mathematical Formulation and Numerical Methods

The numerical model used in this work to simulate the solidification of pure metals and eutectic alloys is the one originally proposed by Swaminathan et al. (1997) and subsequently modified for problems of inverse macro segregation in multicomponent systems (Ferreira et al., 2004).

The model incorporates the following features:

1. Coupled thermo chemical fields it can handle the interaction between temperature and composition fields together with multiple reactions that occur during solidification of multicomponent alloys (e.g., primary phase transformation, phase precipitation, eutectic and peritectic reactions)

DOI: 10.3844/ajeassp.2026.88.116

2. Shrinkage induced flow it accounts for the density difference between the liquid and the primary and secondary solid phases, which gives rise to flow caused by solidification induced shrinkage
3. Temperature rescaling a temperature rescaling technique is employed to treat the solidification of pure and eutectic materials

Model Assumptions

The numerical model for the unsteady solidification of pure metals/compounds and multicomponent alloys is based on the following assumptions (Swaminathan et al., 1997; Ferreira et al., 2004).

Domain

The computational domain is finite and extends along the Z-*axis, i.e.,* $0 \leq Z \leq Z_b$ (see Fig. 1).

- At $Z = 0$, a third-kind (Robin) boundary condition is prescribed for heat flux, while a second-kind (Dirichlet) condition is applied for mass
- At the opposite boundary, $Z = Z_b$, both heat and mass fluxes are zero (insulated/no mass transfer)

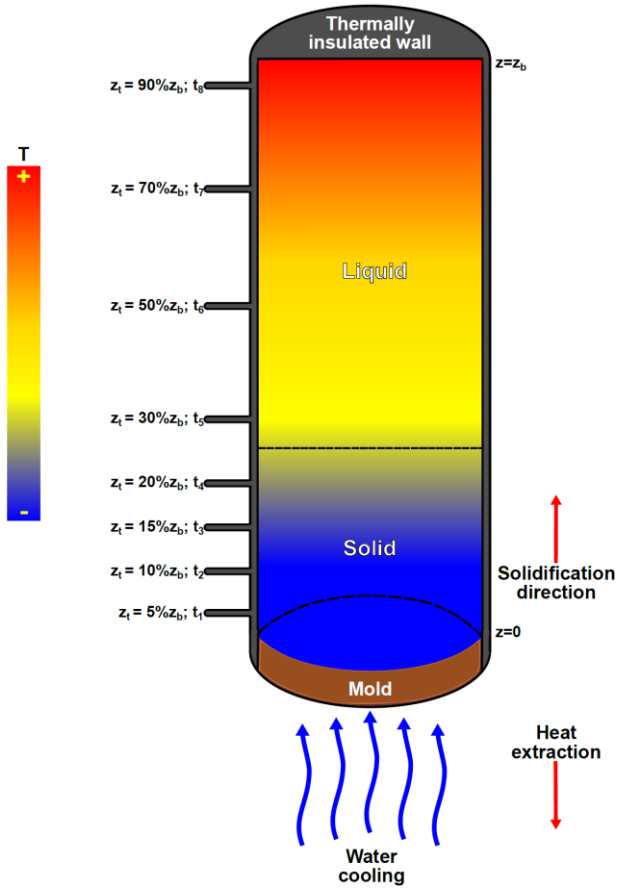

Fig. 1: Schematic representation of transient upward solidification cooled from the bottom

Materials

The phase change material to be solidified is assumed to be either a pure metal (or pure compound) or a multicomponent alloy.

Solid Phase

The solid phase is stationary; once formed, it has zero velocity.

DOI: 10.3844/ajeassp.2026.88.116

Governing Equations

The governing equations for the unsteady solidification of pure metals and eutectic alloys, as given by the analytical solutions in Lipton et al. (1982) and Quaresma et al. (2000) for convective boundary conditions, are as follows:

$$\frac{\partial^2 T_S}{\partial x^2} = \frac{1}{\alpha_S}\frac{\partial T}{\partial t}\ 0 < x < s(t) \tag{1}$$

$$\frac{\partial^2 T_L}{\partial x^2} = \frac{1}{\alpha_l}\frac{\partial T}{\partial t}\ s(t) < x < +\infty \tag{2}$$

$$t = 0,\ 0 < x < +\infty,\ T = T_P \tag{3}$$

$$t > 0,\ x = 0,\ -k\frac{\partial T}{\partial x}\Big|_{x=0} = h(T - T_\infty) \tag{4}$$

$$t > 0,\ x = s(t),\ T = T_F \tag{5}$$

$$t > 0,\ x + \infty,\ T = T_P \tag{6}$$

$$\rho_S L\frac{ds}{dt} = k_S\frac{\partial T}{\partial x}\Big|_{x=^-{}_S} - k_L\frac{\partial T}{\partial x}\Big|_{x=^+{}_S} \tag{7}$$

The thermal variables that influence solidification kinetics and were selected for this comparison are: position versus time, *S(t)*, solid-liquid interface velocity $v = \frac{dS(t)}{dt}$, thermal gradient of the liquid-phase $G_L = \frac{\partial T}{\partial x}\Big|_{x=^+{}_S}$, and cooling rate $\dot{T}_X$ for a given set of Biot numbers.

The reference solution for the solid region is the classic one dimensional solution for a semi-infinite slab whose boundary condition at z = 0 is of the third kind (Trojan, 2014) for non-reactive problems. The temperature profile as a function of time and space can be expressed as:

$$T(x,t) - T_\infty = A_S + B_S\left\{\mathrm{erfc}\left(\frac{x}{2\sqrt{\alpha_S t}}\right) - \exp\left(\frac{h\,x}{k_S} + \frac{h^2\alpha_S t}{k_S^2}\right)\mathrm{erfc}\left(\frac{x}{2\sqrt{\alpha_S t}} + \frac{h\sqrt{\alpha_S\,t}}{k_S}\right)\right\} \tag{8}$$

Where A_S and B_S are constants determined from the solid interface at $s(t) = 0$ and $s(t) = s$.

For $s = 0,\ t > 0$:

$$T_S(s = 0, t) = T_\infty = A_S + B_S \tag{9}$$

This relationship follows from the convective boundary condition that has already been imposed at $x = 0$ for $t > 0$ when deriving the base temperature field $T(x,t)$. Consequently, the condition $T(s = 0, t)$ cannot be imposed on the solid-temperature field $T(x,t)$because no solid exists until a finite time $t^* > 0$has elapsed. In this context, B_S must be determined from the temperature profile at the moving interface $x = s$. Together with the relation $T_\infty = A_S + B_S$, this formulation permits the constants A_S and B_S to be varied freely.

For $x = s$:

$$T_S(x = s, t) = T_F = A_S + B_S\left\{\mathrm{erfc}\left(\frac{s}{2\sqrt{\alpha_S t}}\right) - \exp\left(\frac{h\,s}{k_S} + \frac{h^2\alpha_S t}{k_S^2}\right)\mathrm{erfc}\left(\frac{s}{2\sqrt{\alpha_S t}} + \frac{h\sqrt{\alpha_S\,t}}{k_S}\right)\right\} \tag{10}$$

By introducing the parabolic similarity variable $\frac{s}{2\sqrt{\alpha_S t}}$ and $\varphi(s,t) = \frac{s}{2\sqrt{\alpha_S t}}$, Equation (10) becomes:

$$T_F = A_S + B_S\left\{\mathrm{erfc}(\varphi) - \exp\left(\frac{h\,s}{k_S} + \frac{h^2 s^2}{4\varphi^2 k_S^2}\right)\mathrm{erfc}\left(\varphi + \frac{h\,s}{2\varphi\,k_S}\right)\right\} \tag{11}$$

$$T_\infty = A_S + B_S \tag{12}$$

$$T_F = A_S + B_S\left\{\mathrm{erfc}(\varphi) - \exp\left(\frac{h\,s}{k_S} + \frac{h^2 s^2}{4\varphi^2 k_S^2}\right)\mathrm{erfc}\left(\varphi + \frac{h\,s}{2\varphi\,k_S}\right)\right\} \tag{13}$$

Subtracting Eq. (13) from Eq. (12) leads to:

$$T_\infty - T_F = B_S\left\{1 - \mathrm{erfc}(\varphi) + \exp\left(\frac{h\,s}{k_S} + \frac{h^2 s^2}{4\varphi^2 k_s^2}\right)\mathrm{erfc}\left(\varphi + \frac{h\,s}{2\varphi\,k_S}\right)\right\} \tag{14}$$

Which gives B_S as:

$$B_S = \frac{T_\infty - T_F}{\left\{1 - erfc(\varphi) + exp\left(\frac{h\,s}{k_S} + \frac{h^2 s^2}{4\varphi^2 k_s^2}\right) erfc\left(\varphi + \frac{h\,s}{2\varphi\,k_S}\right)\right\}} \tag{15}$$

Similarly, the constant A_S can be determined as follows:

$$\mathrm{A_S} = \mathrm{T_F} - \frac{(\mathrm{T_\infty} - \mathrm{T_F})}{\left\{1 - \mathrm{erfc}(\varphi) + \exp\left(\frac{\mathrm{h\,s}}{\mathrm{k_S}} + \frac{\mathrm{h^2 s^2}}{4\varphi^2 \mathrm{k_s^2}}\right)\mathrm{erfc}\left(\varphi + \frac{\mathrm{h\,s}}{2\varphi\,\mathrm{k_S}}\right)\right\}}\left\{\mathrm{erfc}(\varphi) - \exp\left(\frac{\mathrm{h\,s}}{\mathrm{k_S}} + \frac{\mathrm{h^2 s^2}}{4\varphi^2 \mathrm{k_s^2}}\right)\mathrm{erfc}\left(\varphi + \frac{\mathrm{h\,s}}{2\varphi\,\mathrm{k_S}}\right)\right\} \tag{16}$$

The temperature profile can now be expressed in terms of constant A_S and B_S:

$$\frac{T_S(x,t) - T_F}{T_\infty - T_F} = \frac{\left\{\mathrm{erfc}\left(\frac{x}{2\sqrt{\alpha_S t}}\right) - \exp\left(\frac{h\,x}{k_S} + \frac{h^2\alpha_S t}{k_s^2}\right)\mathrm{erfc}\left(\frac{x}{2\sqrt{a_S t}} + \frac{h\sqrt{\alpha_S\,t}}{k_S}\right) - \mathrm{erfc}(\varphi) + \exp\left(\frac{h\,s}{k_S} + \frac{h^2 s^2}{4\varphi^2 k_s^2}\right)\mathrm{erfc}\left(\varphi + \frac{h\,s}{2\varphi\,k_S}\right)\right\}}{\left\{1 - \mathrm{erfc}(\varphi) + \exp\left(\frac{h\,s}{k_S} + \frac{h^2 s^2}{4\varphi^2 k_s^2}\right)\mathrm{erfc}\left(\varphi + \frac{h\,s}{2\varphi\,k_S}\right)\right\}} \tag{17}$$

Aiming to express the temperature profile in a more suitable form, the following auxiliary functions $\psi(s,\varphi)$, and $\zeta(s,\varphi)$ can be defined as:

$$\psi(s,t) = \left\{1 - \mathrm{erfc}(\varphi) + \exp\left(\frac{h\,s}{k_S} + \frac{h^2\alpha_S t}{k_s^2}\right)\mathrm{erfc}\left(\varphi + \frac{h\sqrt{\alpha_S\,t}}{k_S}\right)\right\} \tag{18a}$$

$$\psi(s,\varphi) = \left\{1 - \mathrm{erfc}(\varphi) + \exp\left(\frac{h\,s}{k_S} + \frac{h^2 s^2}{4\varphi^2 k_s^2}\right)\mathrm{erfc}\left(\varphi + \frac{h\,s}{2\varphi\,k_S}\right)\right\} \tag{18b}$$

And:

$$\zeta(s,t) = -\mathrm{erfc}(\varphi) + \exp\left(\frac{h\,s}{k_S} + \frac{h^2\alpha_S t}{k_s^2}\right)\mathrm{erfc}\left(\varphi + \frac{h\sqrt{\alpha_S\,t}}{k_S}\right) \tag{19a}$$

$$\zeta(s,\varphi) = -\mathrm{erfc}(\varphi) + \exp\left(\frac{h\,s}{k_S} + \frac{h^2 s^2}{4\varphi^2 k_s^2}\right)\mathrm{erfc}\left(\varphi + \frac{h\,s}{2\varphi\,k_S}\right) \tag{19b}$$

Substituting Eq. (17) and Eq. (18) into Eq. (16) yields:

$$\frac{T_S(x,t) - T_F}{T_\infty - T_F} = \frac{\left\{\mathrm{erfc}\left(\frac{x}{2\sqrt{\alpha_S t}}\right) - \exp\left(\frac{h\,x}{k_S} + \frac{h^2\alpha_S t}{k_s^2}\right)\mathrm{erfc}\left(\frac{x}{2\sqrt{\alpha_S t}} + \frac{h\sqrt{\alpha_S\,t}}{k_S}\right) + \zeta(s,t)\right\}}{\psi(s,t)} \tag{20a}$$

$$\frac{T_S(x,s) - T_F}{T_\infty - T_F} = \frac{\left\{\mathrm{erfc}\left(\varphi\frac{x}{s}\right) - \exp\left(\frac{h\,x}{k_S} + \frac{h^2 s^2}{4\varphi^2 k_s^2}\right)\mathrm{erfc}\left(\varphi\frac{x}{S} + \frac{h\,s}{2\varphi\,k_S}\right) + \zeta(s,\varphi)\right\}}{\psi(s,\varphi)} \tag{20b}$$

The thermal gradient $T_S(x,t)$ *in* the vicinity of boundary $x = {}^{-}s$ is found by deriving the temperature profile with respect to x, which has the following form:

$$\left.\frac{\partial T_S(s,t)}{\partial x}\right|_{x={}^{-}s} = \frac{(T_F - T_\infty)}{\psi(s,t)}\left\{\frac{h}{k_S}\exp\left(\frac{h\,s}{k_S} + \frac{h^2\alpha_S t}{k_s^2}\right)\mathrm{erfc}\left(\varphi + \frac{h\sqrt{\alpha_S\,t}}{k_S}\right) + \frac{2\varphi}{\sqrt{\pi}\,s\exp(\varphi^2)} - \frac{2\varphi}{\sqrt{\pi}\,s\exp\left[\left(\varphi + \frac{h\sqrt{\alpha_S\,t}}{k_S}\right)^2\right]}\exp\left(\frac{h\,s}{k_S} + \frac{h^2\alpha_S t}{k_s^2}\right)\right\} \tag{21a}$$

$$\left.\frac{\partial T_S(s,\varphi)}{\partial x}\right|_{x={}^{-}s} = \frac{(T_F - T_\infty)}{\psi(s,\varphi)}\left\{\frac{h}{k_S}\exp\left(\frac{h\,s}{k_S} + \frac{h^2\,s^2}{4\,\varphi^2\,k_s^2}\right)\mathrm{erfc}\left(\varphi + \frac{h\,s}{2\varphi\,k_S}\right) + \frac{2\varphi}{\sqrt{\pi}\,s\exp(\varphi^2)} - \frac{2\varphi}{\sqrt{\pi}\,s\exp\left[\left(\varphi + \frac{h\,s}{2\varphi\,k_S}\right)^2\right]}\exp\left(\frac{h\,s}{k_S} + \frac{h^2\,s^2}{4\,\varphi^2\,k_s^2}\right)\right\} \tag{21b}$$

A common way to write a solution of a partial differential equation to avoid instability concerning the magnitude of the involved dimensional variables in the function evaluation is to express this in terms of dimensionless numbers with physical meaning, such as Ste, Biot, and $Biot^2Fo$:

$$t = \frac{s^2}{4\alpha_S \varphi^2} \tag{22}$$

$$Fo = \frac{\alpha_S\, t}{s^2} \tag{23}$$

$$Biot = \frac{h\, s}{k_S} \tag{24}$$

$$Ste = \frac{C_{PS}(T_F - T_\infty)}{L} \tag{25}$$

$$Biot^2 Fo = \frac{h^2\, s^2}{4\, \varphi^2\, k_S^2} = \frac{Biot^2}{4\, \varphi^2} \tag{26}$$

$$\psi(Biot, \varphi) = \left\{1 - erfc(\varphi) + exp\left(Biot + \frac{Biot^2}{4\varphi^2}\right) erfc\left(\varphi + \frac{Biot}{2\varphi}\right)\right\} \tag{27}$$

The derivative of s with respect to t gives:

$$\varphi = \frac{s}{2\sqrt{\alpha_S t}} - \frac{h\sqrt{\alpha_S t}}{k_S} \tag{28a}$$

$$s = 2\varphi\sqrt{\alpha_S t} - \frac{2h\alpha_S t}{k_S} \tag{28b}$$

Then the invariant form that modifies the proposed parabolic velocity profile is obtained from Equation (28a); i.e.:

$$\frac{ds}{dt} = \varphi\sqrt{\frac{\alpha_S}{t}} - \frac{2h\alpha_S}{k_S} = \varphi\sqrt{\frac{\alpha_S}{t}} - \Omega \tag{28c}$$

For parabolic velocity, $v = \frac{ds}{dt}$:

$$\Omega = \frac{2h\alpha_S}{k_S} \tag{29d}$$

$$\frac{2\varphi^2\alpha_S}{s} - \frac{2h\alpha_S}{k_S} = \frac{ds}{dt} - \Omega \tag{29e}$$

$$\frac{ds}{dt} - \Omega = \frac{1}{\rho_S L}\left[k_S \frac{\partial T}{\partial x}\Big|_{x=S^-} - k_L \frac{\partial T}{\partial x}\Big|_{x=S^+}\right] \tag{29f}$$

Concerning the liquid phase, the proposed solution is given by:

$$T_L(x,t) = A_L + B_L\left[1 - \text{erf}\left(\frac{x}{2\sqrt{\alpha_L t}}\right)\right] \tag{30}$$

A relationship between the diffusivity of the solid and liquid phases is necessary to assess the similarity variable:

$$n = \sqrt{\frac{\alpha_S}{\alpha_L}} \tag{31}$$

Then, the solution becomes:

$$T_L = (x,t) = A_L + B_L\left[1 - \text{erf}\left(\frac{nx}{2\sqrt{\alpha_S t}}\right)\right] \tag{32}$$

The substitution of initial and boundary conditions into the temperature profiles allows the constants A_L and B_L to be determined:

$$T_L(x = s(t), t) = T_F = A_L + B_L[1 - \text{erf}(n\varphi)] \tag{33}$$

for A_L in $x \to +\infty$, when $t > 0$,

$$T_L(x \to +\infty, t) = T_P = A_L + 0 \ \therefore A_L = T_P \tag{34}$$

$$T_F = T_P + B_L[1 - \text{erf}(n\varphi)] \tag{35}$$

The constant B_L can be determined as:

$$B_L = \frac{T_F - T_P}{1 - \text{erf}(n\varphi)} \tag{36}$$

Finally, after the substitution of constants in the liquid-phase temperature profile, it gives:

$$T_L(x, t) = T_P + \frac{T_F - T_P}{1 - \text{erf}(n\varphi)} \cdot \left[1 - \text{erf}\left(\frac{nx}{2\sqrt{\alpha_S t}}\right)\right] \tag{37}$$

However, by knowing that:

$$\frac{1}{2\sqrt{\alpha_S t}} = \frac{\varphi}{s} \tag{38a}$$

And:

$$\frac{x}{2\sqrt{\alpha_S t}} = \varphi \frac{x}{s} \tag{38b}$$

And combining Eq. (37) and Eq. (38) results in:

$$\frac{T_L(x,t) - T_P}{T_F - T_P} = \theta_L(x, t) = \frac{1}{1 - \text{erf}(n\varphi)} \cdot \left[1 - \text{erf}\left(\frac{nx}{2\sqrt{\alpha_S t}}\right)\right] \tag{39a}$$

$$\frac{T_L(x,s) - T_P}{T_F - T_P} = \theta_L(x, s) = \frac{1}{1 - \text{erf}(n\varphi)} \cdot \left[1 - \text{erf}\left(n\varphi \frac{x}{s}\right)\right] \tag{39b}$$

The derivative of $T_L(x, s)$ with respect to x at $x = s^+$ furnishes the temperature gradient for the liquid phase at the moving interface:

$$\left.\frac{\partial T_L}{\partial x}\right|_{x=s^+} = -\frac{1}{\sqrt{\pi}} \cdot \frac{T_P - T_F}{[1 - \text{erf}(n\varphi)]} \cdot n \cdot \frac{1}{\sqrt{\alpha_S t}} \cdot \exp(-n^2\varphi^2) \tag{40}$$

By inserting the similarity variable φ in Eq. (38):

$$\left.\frac{\partial T_L}{\partial x}\right|_{x=s^+} = -\frac{2\varphi\, n}{\sqrt{\pi}\, s} \cdot \frac{(T_P - T_F)}{\text{erfc}(n\varphi)} \cdot \exp(-n^2\varphi^2) \tag{41}$$

It is important to mention that sometimes the thermal gradient is a function of both the interface position and time, as presented in Eq. (40):

$$\left.\frac{\partial T_L}{\partial x}\right|_{x=s^+} = -\frac{2\varphi\, n}{\sqrt{\pi}\, s} \cdot \frac{(T_P - T_F)}{\text{erfc}\left(n\frac{s}{2\sqrt{\alpha_S t}}\right)} \cdot \exp(-n^2 \frac{s^2}{4\alpha_S t}) \tag{42}$$

By combining Eqs. (20), (27), (38), and (42), the similarity variable can be found:

$$\rho_S L\left(\frac{2\varphi^2\alpha_S}{s}-\Omega\right)=k_S\frac{(T_F-T_\infty)}{\psi(s,\varphi)}\left\{\frac{h}{k_S}\exp\left(\frac{h\,s}{k_S}+\frac{h^2\,s^2}{4\,\varphi^2\,k_S^2}\right)\operatorname{erfc}\left(\varphi+\frac{h\,s}{2\varphi\,k_S}\right)+\frac{2\varphi}{\sqrt{\pi}\,s\exp(\varphi^2)}-\frac{2\varphi}{\sqrt{\pi}\,s\exp\left[\left(\varphi+\frac{h\,s}{2\varphi\,k_S}\right)^2\right]}\exp\left(\frac{h\,s}{k_S}+\frac{h^2\,s^2}{4\,\varphi^2\,k_S^2}\right)\right\}+$$
$$k_L\frac{2\varphi\,n}{\sqrt{\pi}\,s}\cdot\frac{(T_P-T_F)}{\operatorname{erfc}(n\varphi)}\cdot\exp(-n^2\varphi^2) \quad (43)$$

Rearranging the terms in a form for representing heat conduction parameters:

$$\varphi=\frac{C_{PS}\,(T_F-T_\infty)}{L\,\psi(s,\varphi)}\left\{\frac{hs}{2\varphi k_S}\exp\left(\frac{h\,s}{k_S}+\frac{h^2\,s^2}{4\,\varphi^2\,k_S^2}\right)\operatorname{erfc}\left(\varphi+\frac{h\,s}{2\varphi\,k_S}\right)+\frac{1}{\sqrt{\pi}\,\exp(\varphi^2)}\right.$$
$$\left.-\frac{1}{\sqrt{\pi}\,\exp\left[\left(\varphi+\frac{h\,s}{2\varphi\,k_S}\right)^2\right]}\exp\left(\frac{h\,s}{k_S}+\frac{h^2\,s^2}{4\,\varphi^2\,k_S^2}\right)\right\}+\frac{C_{PL}(T_P-T_F)}{L}\,\frac{\alpha_L\rho_L}{\alpha_S\rho_S}\frac{n}{\sqrt{\pi}\,\operatorname{erfc}(n\varphi)\,\exp(n^2\varphi^2)}+\frac{hs}{\varphi\,k_S}\sqrt{\frac{\alpha_S}{t}}$$

And:

$$\varphi=\frac{C_{PS}\,(T_F-T_\infty)}{L\,\psi(s,\varphi)}\left\{\frac{hs}{2\varphi k_S}\exp\left(\frac{h\,s}{k_S}+\frac{h^2\,s^2}{4\,\varphi^2\,k_S^2}\right)\operatorname{erfc}\left(\varphi+\frac{h\,s}{2\varphi\,k_S}\right)+\frac{1}{\sqrt{\pi}\,\exp(\varphi^2)}\right.$$
$$\left.-\frac{1}{\sqrt{\pi}\,\exp\left[\left(\varphi+\frac{h\,s}{2\varphi\,k_S}\right)^2\right]}\exp\left(\frac{h\,s}{k_S}+\frac{h^2\,s^2}{4\,\varphi^2\,k_S^2}\right)\right\}+\frac{C_{PL}(T_P-T_F)}{L}\,\frac{\alpha_L\rho_L}{\alpha_S\rho_S}\frac{n}{\sqrt{\pi}\,\operatorname{erfc}(n\varphi)\,\exp(n^2\varphi^2)}+\Omega$$

In which:

$$N=\frac{\alpha_L\rho_L}{\alpha_S\rho_S} \quad (44)$$

By substituting the dimensionless numbers and heat transfer parameters:

$$\varphi=\frac{Ste_S}{\psi(s,\varphi)}\left\{\frac{Biot}{2\varphi}\exp\left(Biot+\frac{Biot^2}{4\,\varphi^2}\right)\operatorname{erfc}\left(\varphi+\frac{Biot}{2\varphi}\right)+\frac{1}{\sqrt{\pi}\,\exp(\varphi^2)}-\frac{1}{\sqrt{\pi}\,\exp\left[\left(\varphi+\frac{Biot}{2\varphi}\right)^2\right]}\exp\left(Biot+\frac{Biot^2}{4\,\varphi^2}\right)\right\}+$$
$$Ste_L\,N\frac{n}{\sqrt{\pi}\,\operatorname{erfc}(n\varphi)\,\exp(n^2\varphi^2)}+\Omega^* \quad (45)$$

Where $Ste_L=\frac{C_{PL}(T_P-T_F)}{L}$ is the Stefan number considering the liquid phase and, $\Omega^*=\frac{Biot}{\varphi}$ is the dimensionless velocity $\Omega=\frac{2h\alpha_S}{k_S}$:

Solidification Time

The prediction of time for a given solidified layer can be expressed as:

$$t=\gamma s^2+\delta s \quad (46)$$

Where γ is:

$$\gamma=\frac{1}{4\alpha_S\varphi^2} \quad (47)$$

And δ is given as:

$$\delta = \frac{1}{\frac{1}{\rho_S L}\left(k_S \frac{\partial T_S}{\partial x}\Big|_{x=^-_S} - k_L \frac{\partial T_L}{\partial x}\Big|_{x=^+_S}\right)} - 2\gamma s \tag{48}$$

Solid-Liquid Interface Velocity

The interface velocity can be directly derived from the moving boundary differential equation, by making:

$$\frac{s}{2\sqrt{\alpha_S t}} + \frac{h\sqrt{\alpha_S t}}{k_S} = \varphi \tag{49}$$

And, to find the invariable form of velocity correction, we write s as:

$$s = 2\varphi\sqrt{\alpha_S t} - \frac{2h\alpha_S\, t}{k_S} \tag{50}$$

Deriving s with respect to time t gives:

$$\frac{ds}{dt} = \varphi\sqrt{\frac{\alpha_S}{t}} - \frac{2h\alpha_S}{k_S} = \frac{2\varphi^2\alpha_S}{k_S} - \Omega \tag{51}$$

$$v = \frac{ds}{dt} = \frac{1}{\rho_S L}\left(k_S \frac{\partial T_S}{\partial x}\Big|_{x=^-_S} - k_L \frac{\partial T_L}{\partial x}\Big|_{x=^+_S}\right) + \Omega \tag{52}$$

The growth rate v is written in terms of γ and δ provides:

$$v = \frac{1}{2\gamma s + \delta} \tag{53}$$

Thermal gradient of the liquid:
The thermal gradients of the solid and liquid phases are:

$$\frac{\partial T_S(x,s)}{\partial x}\Big|_{x=^-_S} = \frac{(T_F - T_\infty)}{\psi(s,\varphi)}\left\{\frac{h}{k_S}\exp\left(\frac{h\,s}{k_S} + \frac{h^2\,s^2}{4\,\varphi^2\,k_S^2}\right)\operatorname{erfc}\left(\varphi + \frac{h\,s}{2\varphi\,k_S}\right) + \frac{2\varphi}{\sqrt{\pi}\,s\exp(\varphi^2)} - \frac{2\varphi}{\sqrt{\pi}\,s\exp\left[\left(\varphi + \frac{h\,s}{2\varphi\,k_S}\right)^2\right]}\exp\left(\frac{h\,s}{k_S} + \frac{h^2\,s^2}{4\,\varphi^2\,k_S^2}\right)\right\} \tag{54}$$

And:

$$\frac{\partial T_L}{\partial x}\Big|_{x=s^+} = -\frac{1}{\sqrt{\pi}} \cdot \frac{T_P - T_F}{[1-\operatorname{erf}(n\varphi)]} \cdot \frac{n}{\sqrt{\alpha_S t}} \cdot \exp(-n^2\varphi^2) \tag{55}$$

Respectively:

Cooling Rate

The cooling rate can be expressed in terms of the thermal gradient $\frac{\partial T(x,t)}{\partial x}\Big|_{x=^+_S}$ of the liquid phase Eq. (55) and the interface velocity v, Eq. (52):

$$\dot{T}_L = G_L\, v = \frac{\partial T(x,t)}{\partial x}\Big|_{x=^+_S}\frac{dS}{dt} = -\frac{1}{\sqrt{\pi}} \cdot \frac{T_P - T_F}{[1-\operatorname{erf}(n\varphi)]} \cdot \frac{n}{\sqrt{\alpha_S t}} \cdot \exp(-n^2\varphi^2)\left[\frac{1}{\rho_S L}\left(k_S \frac{\partial T_S}{\partial x}\Big|_{x=^-_S} - k_L \frac{\partial T_L}{\partial x}\Big|_{x=^+_S}\right) + \Omega\right] \tag{56}$$

The similarity variable is calculated from the solid-liquid interface thermal balance as:

$$\varphi = \frac{C_{PS}\,(T_F - T_\infty)}{L\,\psi(s,\varphi)}\left\{\frac{hs}{2\varphi k_S}\exp\left(\frac{h\,s}{k_S} + \frac{h^2\,s^2}{4\,\varphi^2\,k_S^2}\right)\operatorname{erfc}\left(\varphi + \frac{h\,s}{2\varphi\,k_S}\right) + \frac{1}{\sqrt{\pi}\,\exp(\varphi^2)} - \frac{1}{\sqrt{\pi}\,\exp\left[\left(\varphi + \frac{h\,s}{2\varphi\,k_S}\right)^2\right]}\exp\left(\frac{h\,s}{k_S} + \frac{h^2\,s^2}{4\,\varphi^2\,k_S^2}\right)\right\} +$$
$$\frac{C_{PL}(T_P - T_F)}{L}\,\frac{\alpha_L\rho_L}{\alpha_S\rho_S}\frac{n}{\sqrt{\pi}\,\operatorname{erfc}(n\varphi)\,\exp(n^2\varphi^2)} + \Omega \tag{57}$$

The set of equations from the analytical solution for transient solidification proposed by Clyne and Garcia (1980). necessary to calculate the thermal variables is the following:

Solidification Time

The prediction of time for a given solidified layer can be expressed as:

$$t = \alpha S^2 + \beta S \tag{58}$$

where α and β are defined as:

$$\alpha = \frac{1}{4\, a_S\, \phi^2} \tag{59}$$

And:

$$\beta = \frac{c_{PS}\ L}{\sqrt{\pi}\ \phi \exp(\phi^2)\ [M+\mathrm{erf}(\phi)]h_i} \tag{60}$$

Respectively. In Eq. (59), a_S represents the diffusivity of the solid, and ϕ the similarity variable used in Garcia et al.'s model. When the mold is not considered, as in this study, where $M = 0$, the mean interfacial heat transfer coefficient h_i becomes equal to the mean global heat transfer coefficient h, i.e., $h = h_i$. The specific heat and density of the solid phase are denoted by c_{PS} and c_{PS}, respectively.

Solid-Liquid Interface Velocity

The solid-liquid interface velocity can be directly derived from the moving boundary differential equation, Eq. (7), or by the derivative of Eq. (8), as deduced by Garcia et al. (1978); (1979) Clyne et al. (1980):

$$\frac{1}{v} = \frac{dt}{dS} = 2\alpha S + \beta \tag{61}$$

And, by v provides:

$$v = \frac{dS}{dt} = \frac{1}{2\alpha S+\beta} \tag{62}$$

Thermal gradient of the liquid:

One simple form to compute the thermal gradient is by taking the temperature profile of the liquid and deriving it with respect to: $G_L = \left.\frac{\partial T(x,t)}{\partial x}\right|_{x=^+S}$:

$$G_L = \left.\frac{\partial T(x,t)}{\partial x}\right|_{x=^+S} = \frac{2n\phi(T_P-T_F)}{\sqrt{\pi}\,\mathrm{erfc}(n\phi)\exp(n^2\phi^2)(S+S_0)} \tag{63}$$

Cooling Rate

The cooling rate can be expressed in terms of the thermal gradient $\left.\frac{\partial T(x,t)}{\partial x}\right|_{x=^+S}$ and the interface velocity v:

$$\dot{T}_L = G_L\, v = \left.\frac{\partial T(x,t)}{\partial x}\right|_{x=^+S}\frac{dS}{dt} = \frac{2n\phi(T_P-T_F)}{\sqrt{\pi}\,\mathrm{erfc}(n\phi)\exp(n^2\phi^2)(S+S_0)}\,\frac{1}{2\alpha S+\beta} \tag{64}$$

The similarity variable is calculated from the solid-liquid interface thermal balance as:

$$\frac{\exp(-\phi^2)}{M+\mathrm{erf}(\phi)} - \frac{m(T_V-T_F)\exp(-n^2\phi^2)}{(T_F-T_P)[1-\mathrm{erf}(n\phi)]} - \sqrt{\pi}\,\phi\,\frac{L}{c_{PS}(T_F-T_0)} = 0 \tag{65}$$

Experimental Procedure

The eutectic alloy was prepared from commercially pure solvent Al ≅ 99.7% and solute Si ≅ 99.5%, determined through a stoichiometric calculation based on the desired eutectic composition (Al-12.6 wt.%Si), and on the volume of the mold. The checking of the nominal compositions of Al and Si elements was carried out utilizing a thermal characterization, which consisted of the insertion in the liquid metal of type K thermocouples connected to a temperature recorder. The resulting experimental curve furnishes the eutectic temperature ($T_{Eut} = 577°C$). A comprehensive description of the experimental procedure can be found in Rocha et al. (202); Swaminathan et al. (1997); Ferreira et al. (2004).

Figure 2 shows a scheme of the upward unsteady directional solidification device used in the experiment to obtain the thermal data and the as-cast ingot. The thermocouples were positioned at 5, 10, 15, 20, 30, 50, 70, and 90 mm from the heat-extracting surface and calibrated at the melting point of aluminum. Solidification occurred primarily through a water-

DOI: 10.3844/ajeassp.2026.88.116

cooled bottom, driving upward directional growth, as shown in Figure 3. A stainless-steel mold, with 60 mm internal diameter, 160 mm height, and 5 mm wall thickness, was employed. An insulating alumina layer covered the inner vertical surface to minimize radial heat loss, while an insulated top cover reduced heat transfer from the metal to air, minimizing both radiation and convection. The bottom of the mold was sealed with a thin (3 mm) carbon steel sheet featuring a roughness of approximately 35 μm. The investigated alloy was melted in situ, and the lateral electric heaters' power was precisely controlled to achieve the target superheat at the 5 mm thermocouple. Solidification commenced upon disconnecting the electric heaters and simultaneously initiating water flow of 7 l/s at 298.15K.

Figure 2. Schematic representation of upward-directional solidification mold and thermocouple positions.

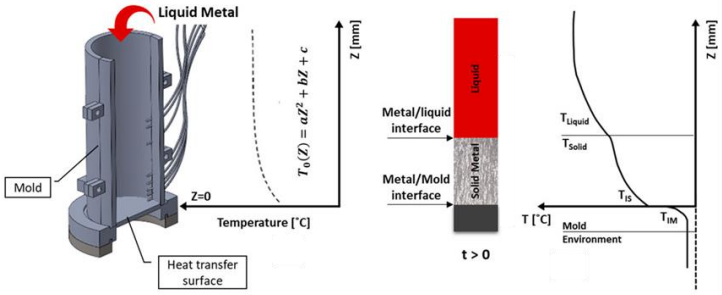

Fig. 2: Schematic representation of upward-directional solidification mold and thermocouple positions

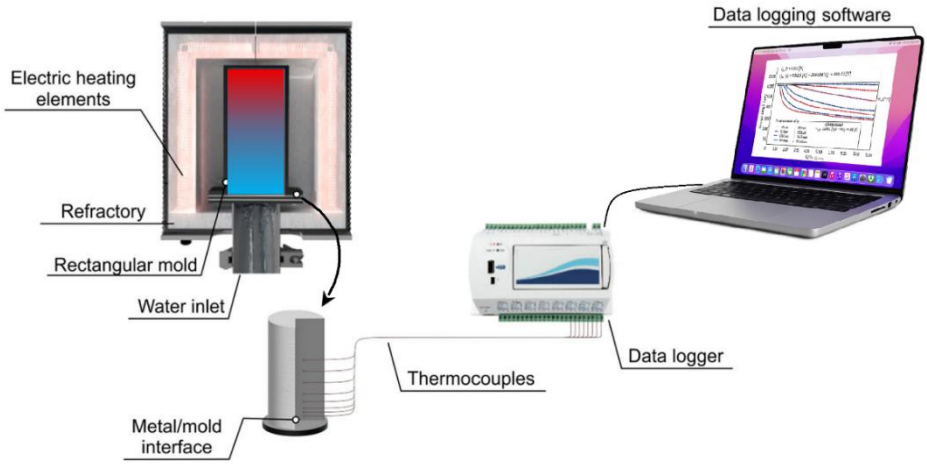

Fig. 3: Schematic representation of upward-directional solidification apparatus.

Results and Discussion

The thermal variables are calculated for Al, Cu, Fe, Pb, Sn, and Ni with the aim of analyzing the results obtained by a classical (Clyne and Garcia, 1980) and a recently published analytical model for solidification (Santos, 2024). The comparison was made by evaluating isothermal position, velocity, thermal gradient, and cooling rate for a set of Biot numbers, considering 4% melt superheat.

The analytical model is initially compared against the numerical model for transient multicomponent alloy solidification (Ivaldo et al., 2025; Swaminathan et al., 1997; Ferreira et al., 2004) and experimental data from (Rocha et al., 2020). The numerical model was used to find solutions for all available thermocouple positions. Figure 4 presents the numerical simulation of Al-12.6 wt%Si, illustrating key kinetic variables including temperature profiles, solid-liquid interface position versus time, velocity, thermal gradient, and cooling rate. During external calculation of the global mean heat transfer coefficient, $\overline{\overline{h}}$, using integral methods, we have integrated $h(t)$ to obtain its mean integral value: $\bar{h} =$

$\frac{1}{t_\infty}\int_0^{t_\infty} h(t)dt$, where $t_\infty \to +\infty$ is significantly greater than the process time $t = 400\ s$, i.e., $t_\infty = 60000000$ s is enough to converge the thermal gradient and cooling rate. In the case of Clyne and Garcia's solution, $t_\infty = 400\ s$.

Figure 5 shows the solidification related thermal variables solid–liquid interface velocity, cooling rate, and thermal gradient—plotted versus the distance from the chill for the analytical solution, the experimental data reported in [40], and the numerical simulation. The excellent agreement between the experimental results and the analytical solution provides strong validation of the analytical model. Notably, the numerical simulation shows improved agreement with the experiments, especially concerning the solid–liquid interface velocity. Although the overall model is validated, additional experimental data would be valuable for further refining our understanding of this interfacial behaviour.

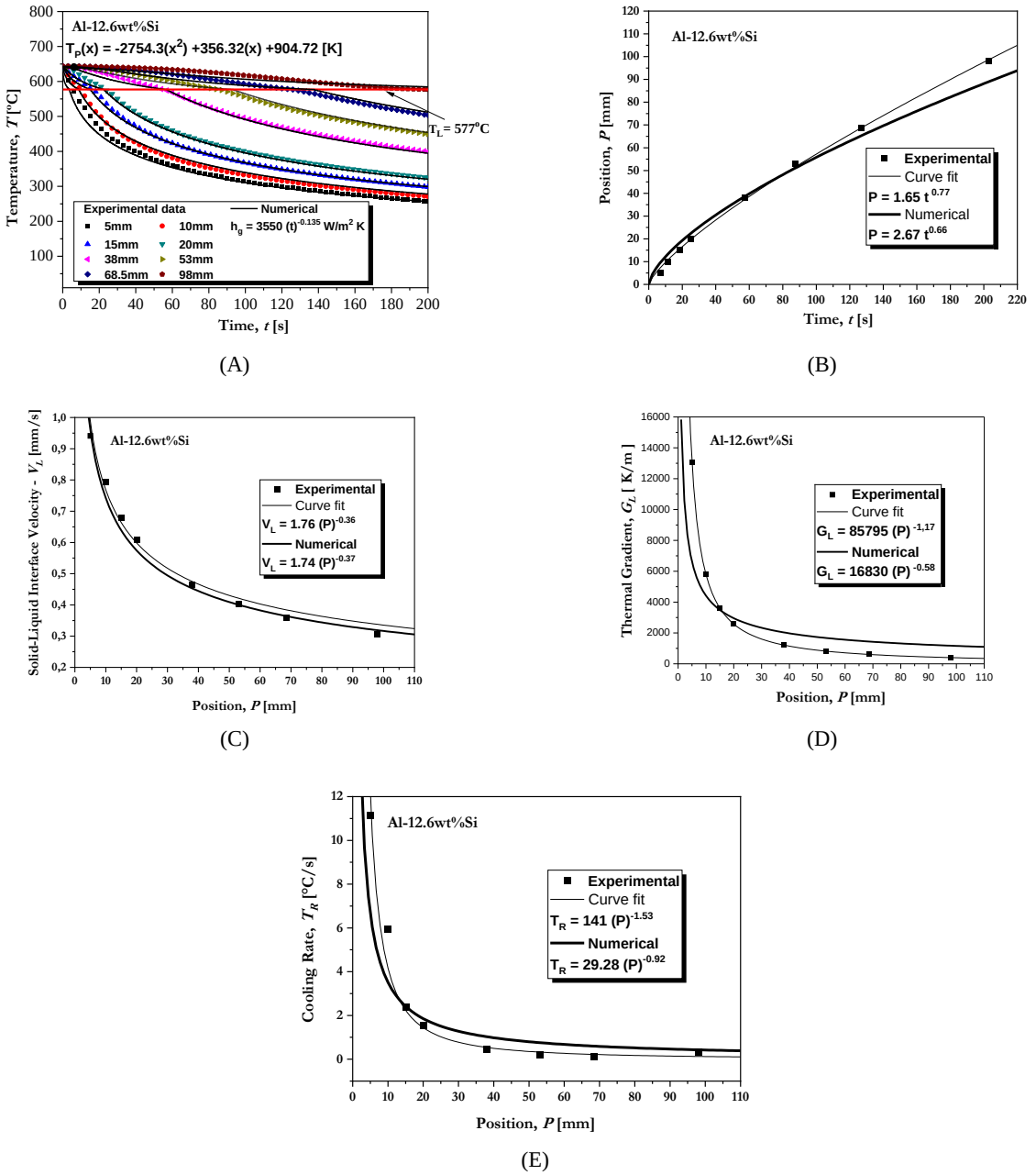

Fig. 4: Numerical predictions against experimental data for thermal variables: (A) cooling curves, (B) position versus time, (C) solid/liquid interface velocity, (D) cooling rate, and (E) thermal gradient

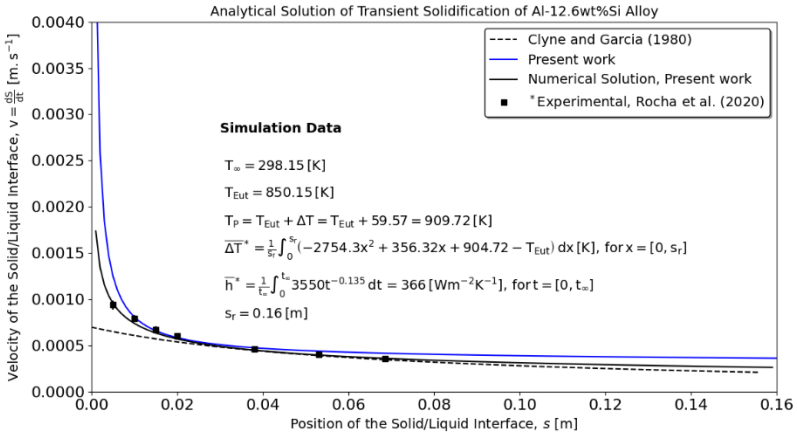

(A)

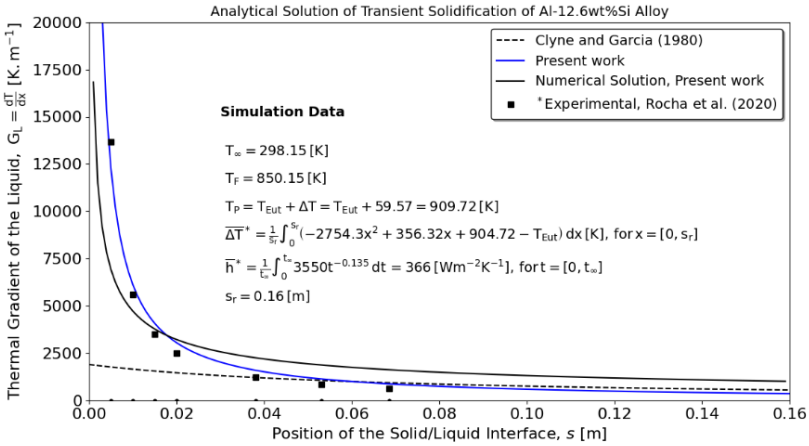

(B)

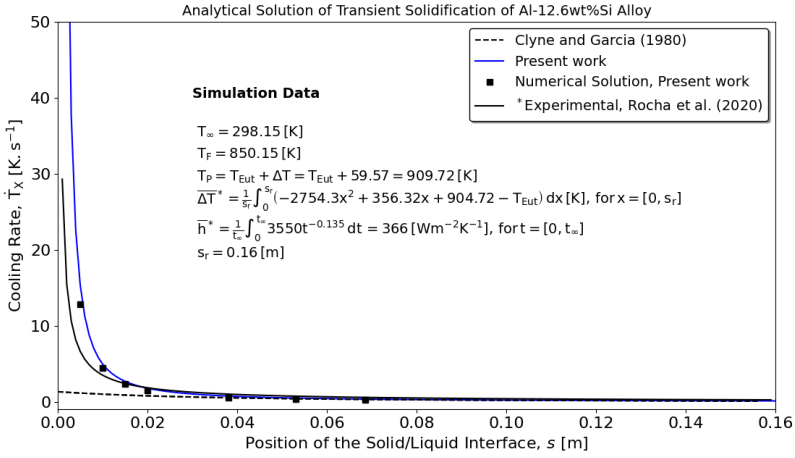

(C)

Fig. 5: Analytical and numerical predictions compared to experimental data for thermal variables as a function of position from the chill: (A) solid/liquid interface velocity, (B) cooling rate, and (C) thermal gradient

Figure 6 shows the solid–liquid interface velocity (growth rate) as a function of position. Both models produce very similar predictions over the whole range of Biot numbers considered, accurately capturing the interface velocity for all of the investigated materials. However, the new model predicts steeper interface velocities than the classical solution in regions of high Biot number and fast flow, where the classical solution yields smoother curves. Equation (52) employs a liquid thermal gradient that is similar to the one used in Equation (62), but it also incorporates a second term representing the solid thermal gradient. This additional term, which uses a new similarity variable, generates a steeper thermal gradient.

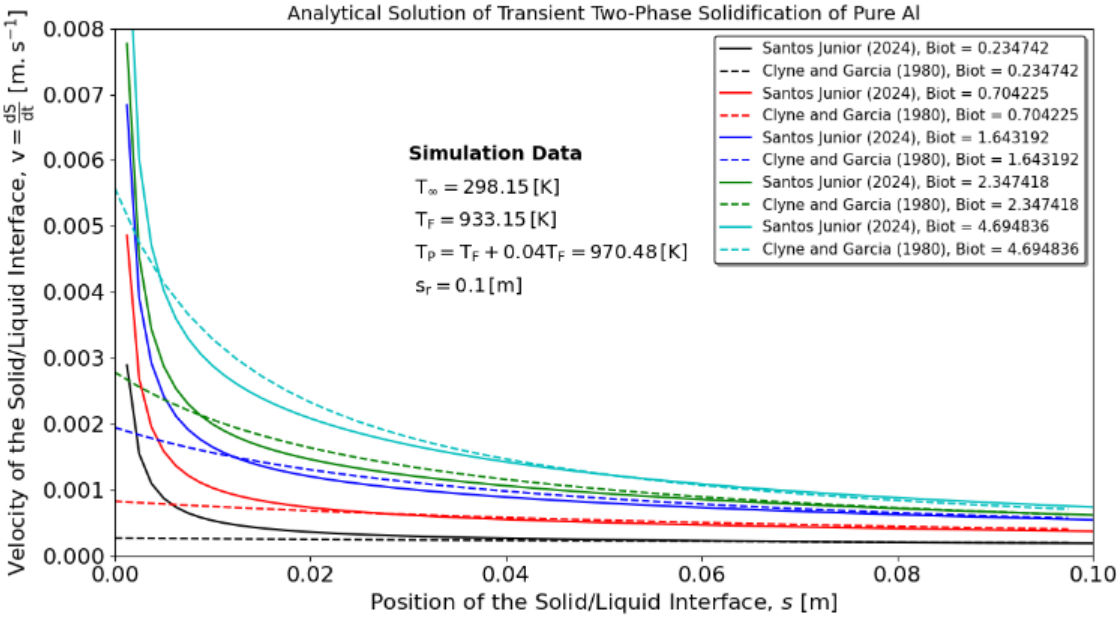

(A)

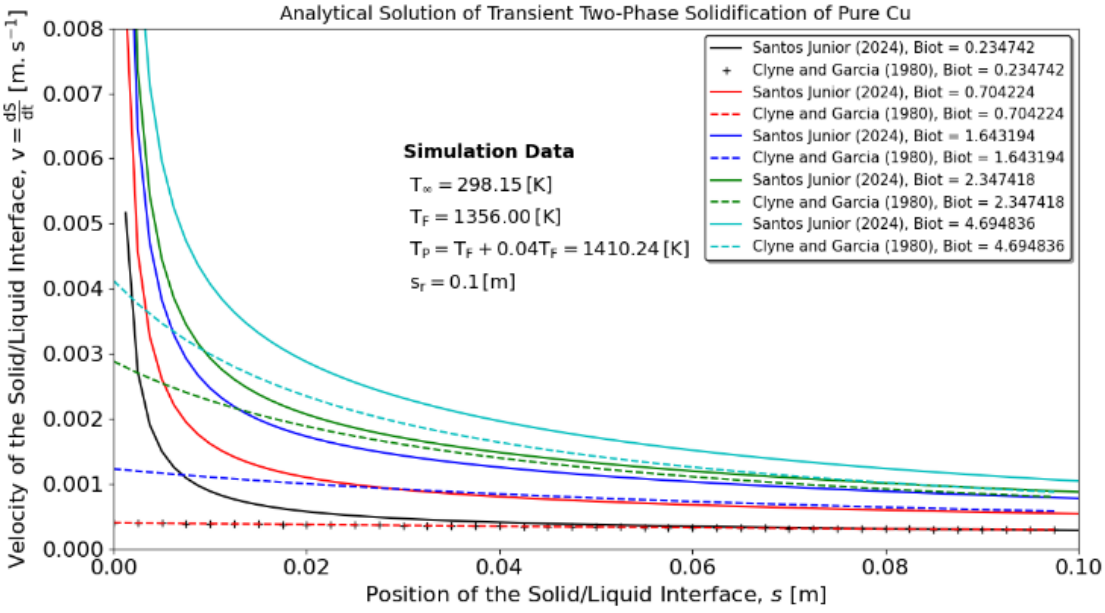

(B)

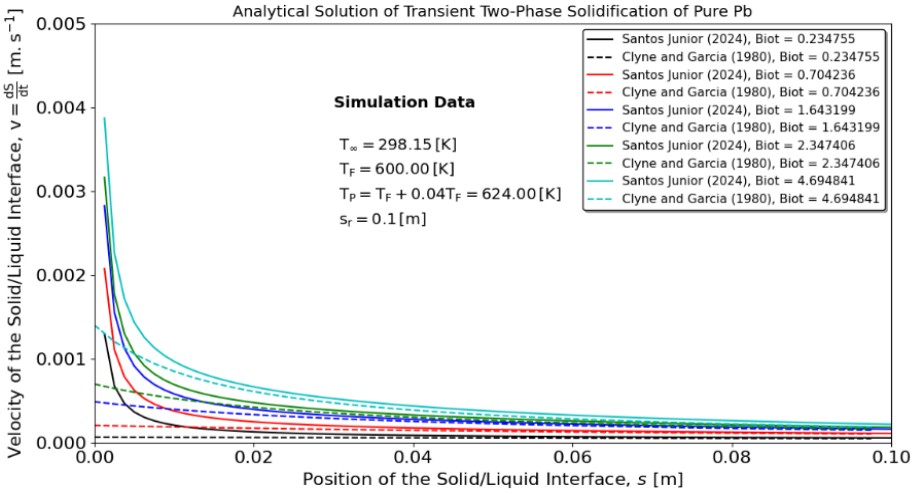
Analytical Solution of Transient Two-Phase Solidification of Pure Pb
Simulation Data
$T_\infty = 298.15\,[K]$
$T_F = 600.00\,[K]$
$T_P = T_F + 0.04T_F = 624.00\,[K]$
$s_r = 0.1\,[m]$
Santos Junior (2024), Biot = 0.234755
Clyne and Garcia (1980), Biot = 0.234755
Santos Junior (2024), Biot = 0.704236
Clyne and Garcia (1980), Biot = 0.704236
Santos Junior (2024), Biot = 1.643199
Clyne and Garcia (1980), Biot = 1.643199
Santos Junior (2024), Biot = 2.347406
Clyne and Garcia (1980), Biot = 2.347406
Santos Junior (2024), Biot = 4.694841
Clyne and Garcia (1980), Biot = 4.694841
Velocity of the Solid/Liquid Interface, $v = \frac{dS}{dt}$ [m. s^{-1}]
Position of the Solid/Liquid Interface, s [m]

(C)

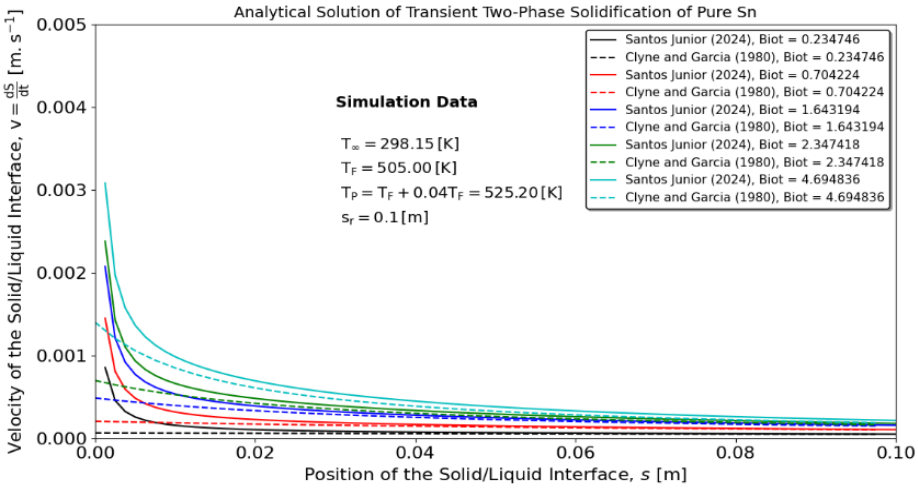
Analytical Solution of Transient Two-Phase Solidification of Pure Sn
Simulation Data
$T_\infty = 298.15\,[K]$
$T_F = 505.00\,[K]$
$T_P = T_F + 0.04T_F = 525.20\,[K]$
$s_r = 0.1\,[m]$
Santos Junior (2024), Biot = 0.234746
Clyne and Garcia (1980), Biot = 0.234746
Santos Junior (2024), Biot = 0.704224
Clyne and Garcia (1980), Biot = 0.704224
Santos Junior (2024), Biot = 1.643194
Clyne and Garcia (1980), Biot = 1.643194
Santos Junior (2024), Biot = 2.347418
Clyne and Garcia (1980), Biot = 2.347418
Santos Junior (2024), Biot = 4.694836
Clyne and Garcia (1980), Biot = 4.694836
Velocity of the Solid/Liquid Interface, $v = \frac{dS}{dt}$ [m. s^{-1}]
Position of the Solid/Liquid Interface, s [m]

(D)

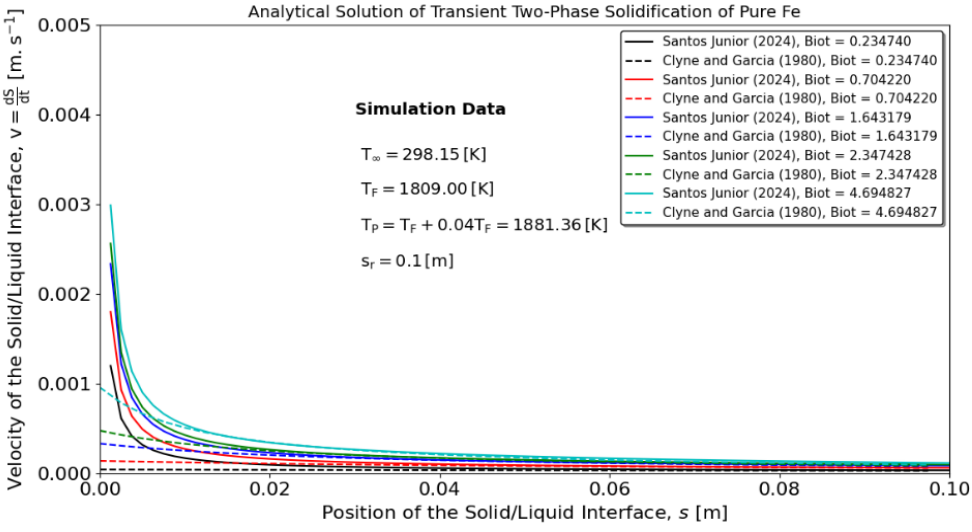
Analytical Solution of Transient Two-Phase Solidification of Pure Fe
Simulation Data
$T_\infty = 298.15\,[K]$
$T_F = 1809.00\,[K]$
$T_P = T_F + 0.04T_F = 1881.36\,[K]$
$s_r = 0.1\,[m]$
Santos Junior (2024), Biot = 0.234740
Clyne and Garcia (1980), Biot = 0.234740
Santos Junior (2024), Biot = 0.704220
Clyne and Garcia (1980), Biot = 0.704220
Santos Junior (2024), Biot = 1.643179
Clyne and Garcia (1980), Biot = 1.643179
Santos Junior (2024), Biot = 2.347428
Clyne and Garcia (1980), Biot = 2.347428
Santos Junior (2024), Biot = 4.694827
Clyne and Garcia (1980), Biot = 4.694827
Velocity of the Solid/Liquid Interface, $v = \frac{dS}{dt}$ [m. s^{-1}]
Position of the Solid/Liquid Interface, s [m]

(E)

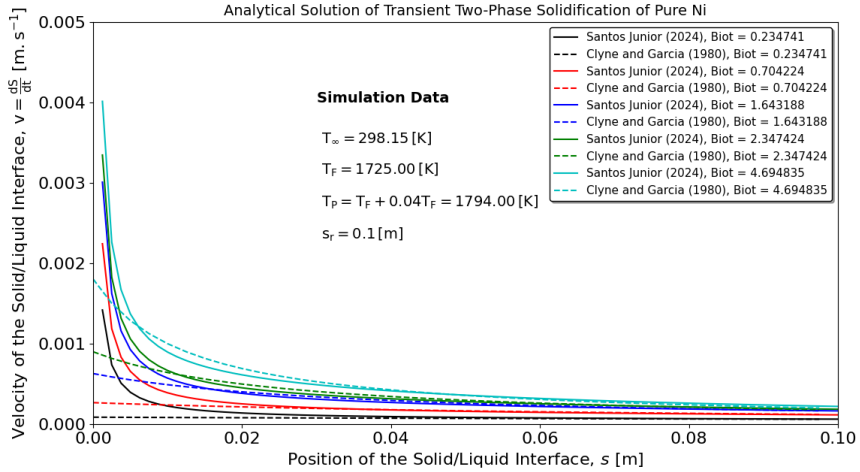

(F)

Fig. 6: Analytical predictions for the solid-liquid interface velocity versus time for pure: (A) Al, (B) Cu, (C) Pb, (D) Sn, (E) Fe, and (F) Ni

The thermal gradient of the liquid phase is plotted against the solid-liquid interface position, as shown in Figure 7. For all cases analyzed, the predicted thermal gradient by the new approach is steeper than that furnished by the classical model, whose differences can be achieved up to 8 times. As thermal gradients are inherently steeper in nature, this can also be observed in experimental transient solidification studies (Rocha et al., 2020). Consequently, it appears that the classical model may not be as accurate for calculating the thermal gradient. The differences in solutions arise from the combined effect of the new similarity variable, which accounts for parabolic and linear profiles calculated at the moving boundary interface via energy balance. While this approach provides valuable insights, a general solution for this type of problem might be based on a full quadratic profile.

Figure 7 shows the liquid phase thermal gradient plotted as a function of the solid–liquid interface position. For every case examined, the gradient predicted with the new approach is noticeably steeper than that given by the classical model up to eight fold larger in some instances. Because thermal gradients are intrinsically steep, this behaviour is also observed in experimental transient solidification studies (Rocha et al., 2020). Consequently, the classical model may be insufficiently accurate for calculating the thermal gradient.

The disparity between the two solutions stems from the new similarity variable, which incorporates both parabolic and linear temperature profiles at the moving interface as imposed by the energy balance condition. Although this approach yields valuable insight, a more general solution for this class of problems could be obtained by adopting a full quadratic temperature profile.

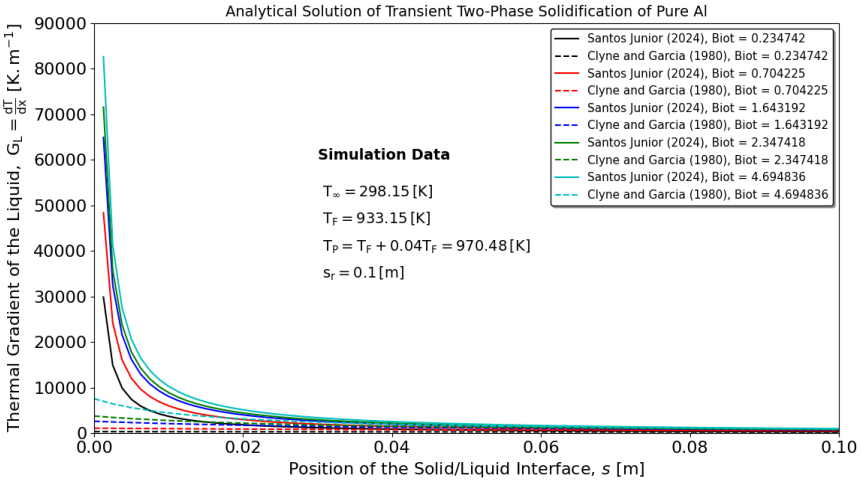

(A)

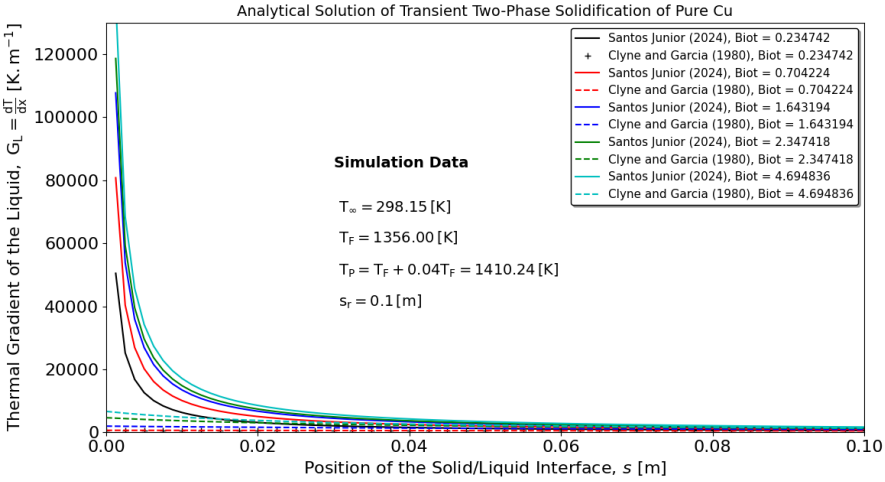
Analytical Solution of Transient Two-Phase Solidification of Pure Cu
Thermal Gradient of the Liquid, $G_L = \frac{dT}{dx}$ [K. m^{-1}]
Position of the Solid/Liquid Interface, s [m]
Simulation Data
$T_\infty = 298.15$ [K]
$T_F = 1356.00$ [K]
$T_P = T_F + 0.04T_F = 1410.24$ [K]
$s_r = 0.1$ [m]
Santos Junior (2024), Biot = 0.234742
Clyne and Garcia (1980), Biot = 0.234742
Santos Junior (2024), Biot = 0.704224
Clyne and Garcia (1980), Biot = 0.704224
Santos Junior (2024), Biot = 1.643194
Clyne and Garcia (1980), Biot = 1.643194
Santos Junior (2024), Biot = 2.347418
Clyne and Garcia (1980), Biot = 2.347418
Santos Junior (2024), Biot = 4.694836
Clyne and Garcia (1980), Biot = 4.694836

(B)

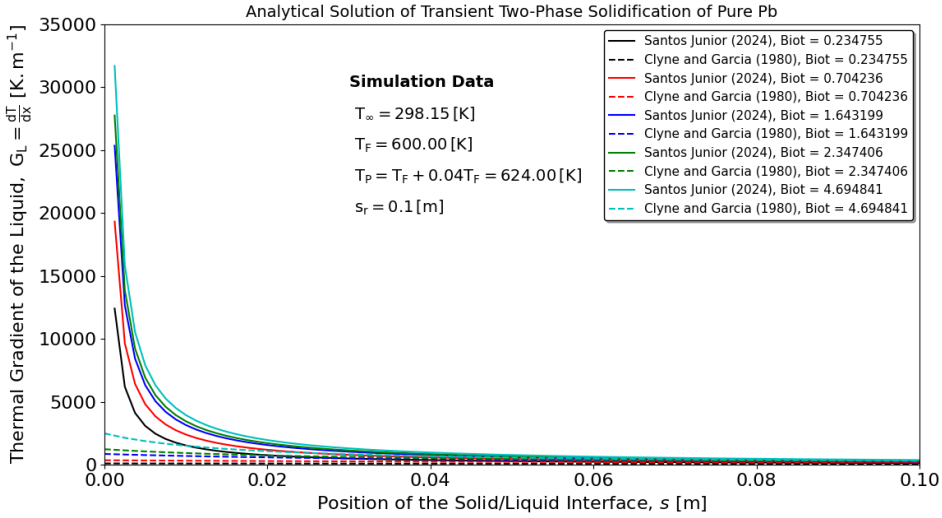
Analytical Solution of Transient Two-Phase Solidification of Pure Pb
Thermal Gradient of the Liquid, $G_L = \frac{dT}{dx}$ [K. m^{-1}]
Position of the Solid/Liquid Interface, s [m]
Simulation Data
$T_\infty = 298.15$ [K]
$T_F = 600.00$ [K]
$T_P = T_F + 0.04T_F = 624.00$ [K]
$s_r = 0.1$ [m]
Santos Junior (2024), Biot = 0.234755
Clyne and Garcia (1980), Biot = 0.234755
Santos Junior (2024), Biot = 0.704236
Clyne and Garcia (1980), Biot = 0.704236
Santos Junior (2024), Biot = 1.643199
Clyne and Garcia (1980), Biot = 1.643199
Santos Junior (2024), Biot = 2.347406
Clyne and Garcia (1980), Biot = 2.347406
Santos Junior (2024), Biot = 4.694841
Clyne and Garcia (1980), Biot = 4.694841

(C)

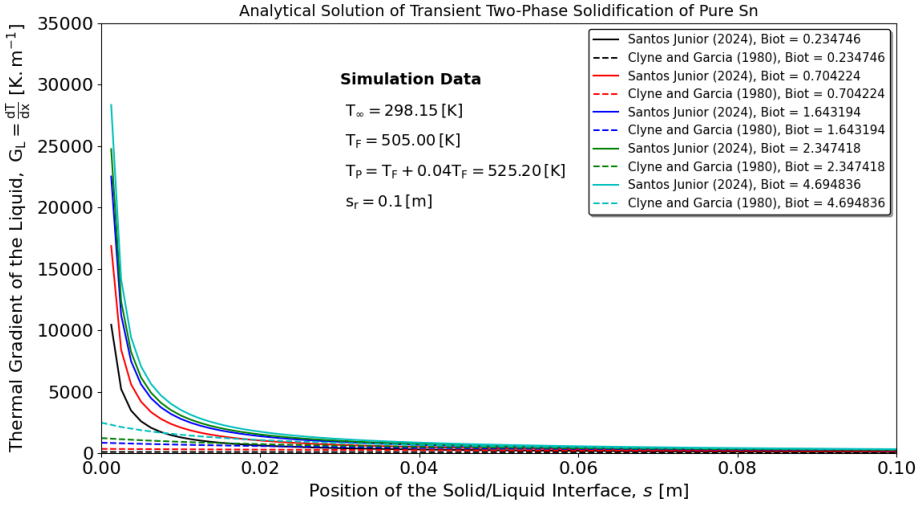
Analytical Solution of Transient Two-Phase Solidification of Pure Sn
Thermal Gradient of the Liquid, $G_L = \frac{dT}{dx}$ [K. m^{-1}]
Position of the Solid/Liquid Interface, s [m]
Simulation Data
$T_\infty = 298.15$ [K]
$T_F = 505.00$ [K]
$T_P = T_F + 0.04T_F = 525.20$ [K]
$s_r = 0.1$ [m]
Santos Junior (2024), Biot = 0.234746
Clyne and Garcia (1980), Biot = 0.234746
Santos Junior (2024), Biot = 0.704224
Clyne and Garcia (1980), Biot = 0.704224
Santos Junior (2024), Biot = 1.643194
Clyne and Garcia (1980), Biot = 1.643194
Santos Junior (2024), Biot = 2.347418
Clyne and Garcia (1980), Biot = 2.347418
Santos Junior (2024), Biot = 4.694836
Clyne and Garcia (1980), Biot = 4.694836

(D)

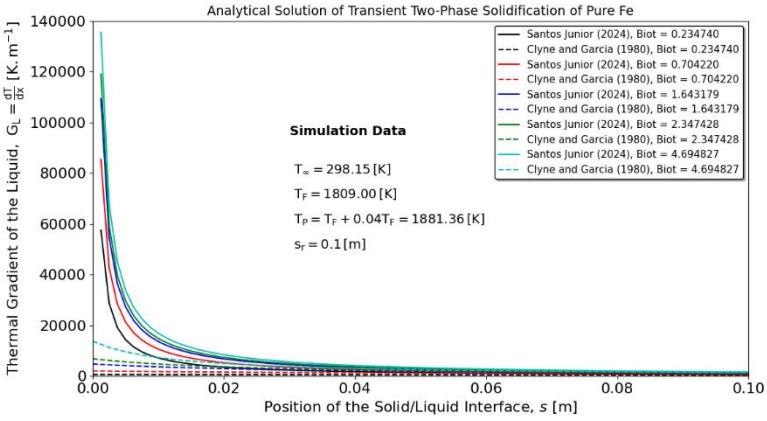

(E)

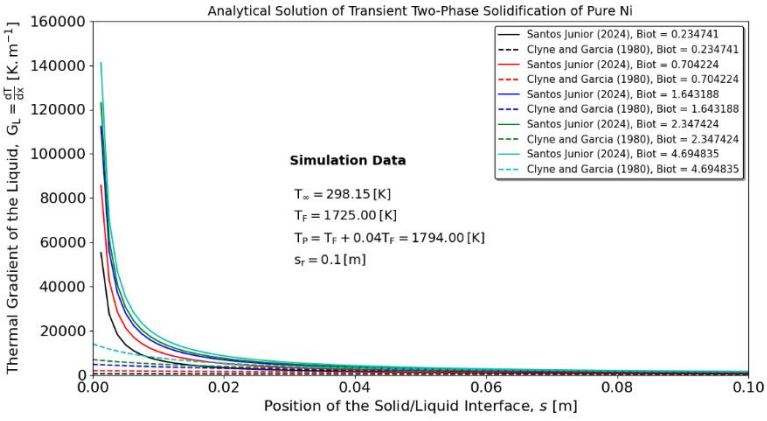

(F)

Fig. 7: Analytical predictions of the thermal gradient of the liquid phase versus time for pure: (A) Al, (B) Cu, (C) Pb, (D) Sn, (E) Fe, and (F) Ni

Figure 8 presents the cooling rate as a function of the solid–liquid interface position for several Biot numbers. All cases display a comparable trend, indicating that the classical model underestimates the steepness of the cooling rate when compared with the experimental measurements reported in Rocha et al. (2020). Equation (64) for transient solidification, $\dot{T}_L = \frac{dx}{/dt} v_L$,, shows that the cooling rate scales with the interface velocity; therefore, a steep cooling rate is expected for the velocities observed. Although the solid liquid interface velocities predicted by the classical and the new models are essentially identical, the new formulation through its modified treatment of the temperature gradient produces a markedly steeper cooling rate, in line with the experimental data.

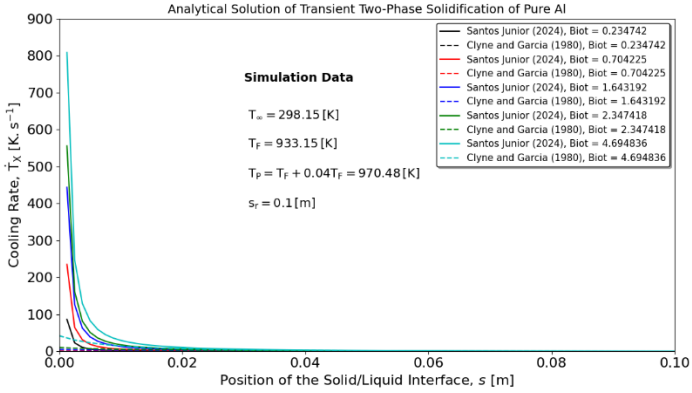

(A)

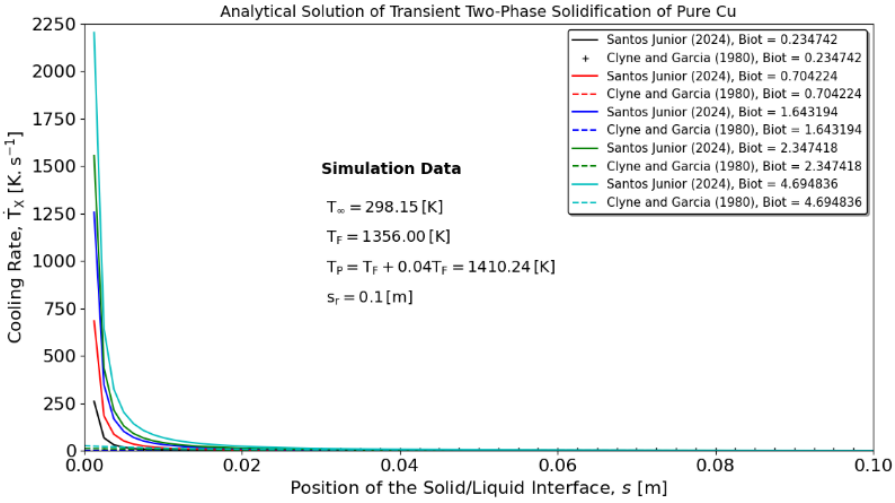
Analytical Solution of Transient Two-Phase Solidification of Pure Cu
Simulation Data
$T_\infty = 298.15\,[K]$
$T_F = 1356.00\,[K]$
$T_P = T_F + 0.04T_F = 1410.24\,[K]$
$s_r = 0.1\,[m]$
Santos Junior (2024), Biot = 0.234742
Clyne and Garcia (1980), Biot = 0.234742
Santos Junior (2024), Biot = 0.704224
Clyne and Garcia (1980), Biot = 0.704224
Santos Junior (2024), Biot = 1.643194
Clyne and Garcia (1980), Biot = 1.643194
Santos Junior (2024), Biot = 2.347418
Clyne and Garcia (1980), Biot = 2.347418
Santos Junior (2024), Biot = 4.694836
Clyne and Garcia (1980), Biot = 4.694836
Cooling Rate, $\dot{T}_X$ [K. s^{-1}]
Position of the Solid/Liquid Interface, s [m]

(B)

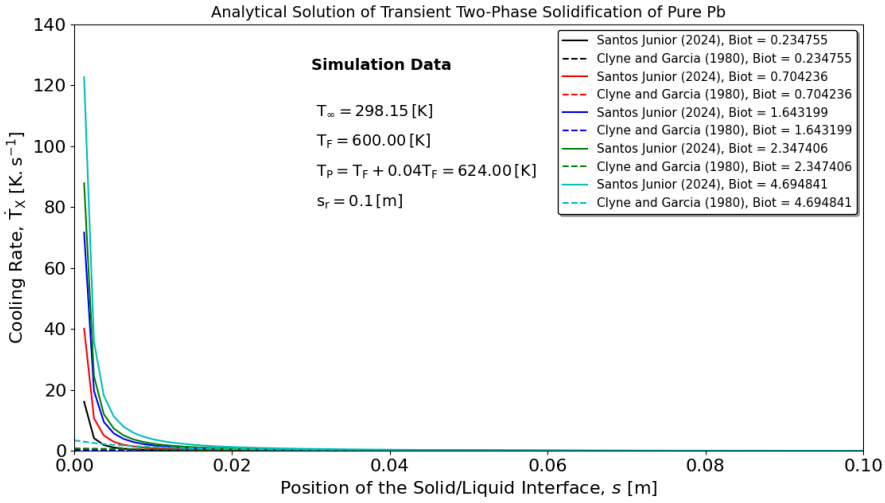
Analytical Solution of Transient Two-Phase Solidification of Pure Pb
Simulation Data
$T_\infty = 298.15\,[K]$
$T_F = 600.00\,[K]$
$T_P = T_F + 0.04T_F = 624.00\,[K]$
$s_r = 0.1\,[m]$
Santos Junior (2024), Biot = 0.234755
Clyne and Garcia (1980), Biot = 0.234755
Santos Junior (2024), Biot = 0.704236
Clyne and Garcia (1980), Biot = 0.704236
Santos Junior (2024), Biot = 1.643199
Clyne and Garcia (1980), Biot = 1.643199
Santos Junior (2024), Biot = 2.347406
Clyne and Garcia (1980), Biot = 2.347406
Santos Junior (2024), Biot = 4.694841
Clyne and Garcia (1980), Biot = 4.694841
Cooling Rate, $\dot{T}_X$ [K. s^{-1}]
Position of the Solid/Liquid Interface, s [m]

(C)

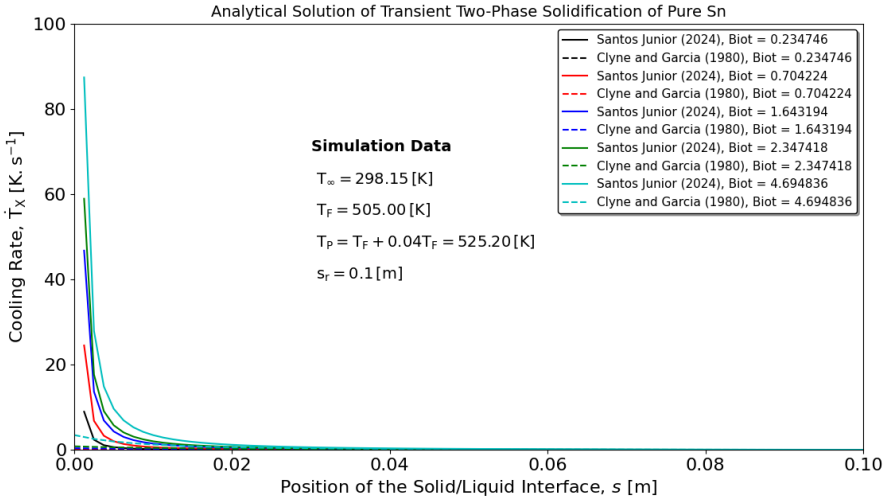
Analytical Solution of Transient Two-Phase Solidification of Pure Sn
Simulation Data
$T_\infty = 298.15\,[K]$
$T_F = 505.00\,[K]$
$T_P = T_F + 0.04T_F = 525.20\,[K]$
$s_r = 0.1\,[m]$
Santos Junior (2024), Biot = 0.234746
Clyne and Garcia (1980), Biot = 0.234746
Santos Junior (2024), Biot = 0.704224
Clyne and Garcia (1980), Biot = 0.704224
Santos Junior (2024), Biot = 1.643194
Clyne and Garcia (1980), Biot = 1.643194
Santos Junior (2024), Biot = 2.347418
Clyne and Garcia (1980), Biot = 2.347418
Santos Junior (2024), Biot = 4.694836
Clyne and Garcia (1980), Biot = 4.694836
Cooling Rate, $\dot{T}_X$ [K. s^{-1}]
Position of the Solid/Liquid Interface, s [m]

(D)

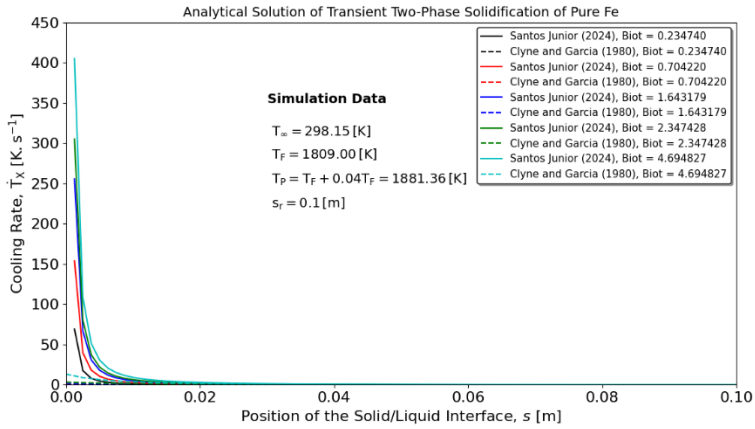

(E)

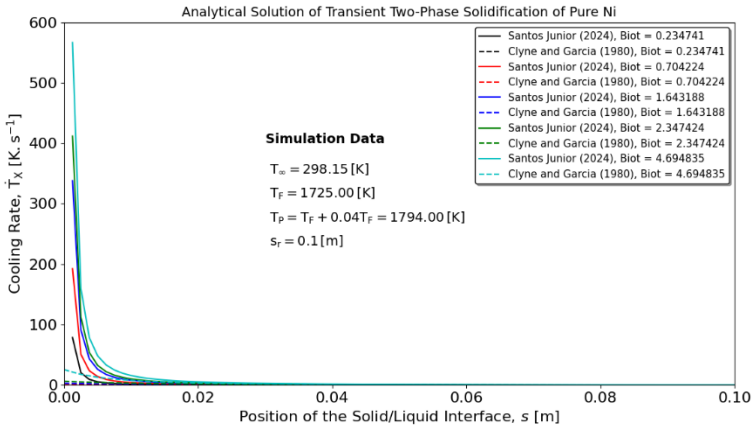

(F)

Fig. 8: Analytical predictions of the cooling rate against time for pure: (A) Al, (B) Cu, C(C) Pb, (D) Sn, (E) Fe, and (F) Ni

The final application of this analytical model is a comparison with a classical solidification model for pure and eutectic materials (Garcia et al., 1979; Clyne and Garcia, 1980). This analysis involves freezing water at an altitude of 5000 m to capture the surface thermal gradient. The present model can accommodate a wide range of Biot numbers, as shown in Figures 9-11.

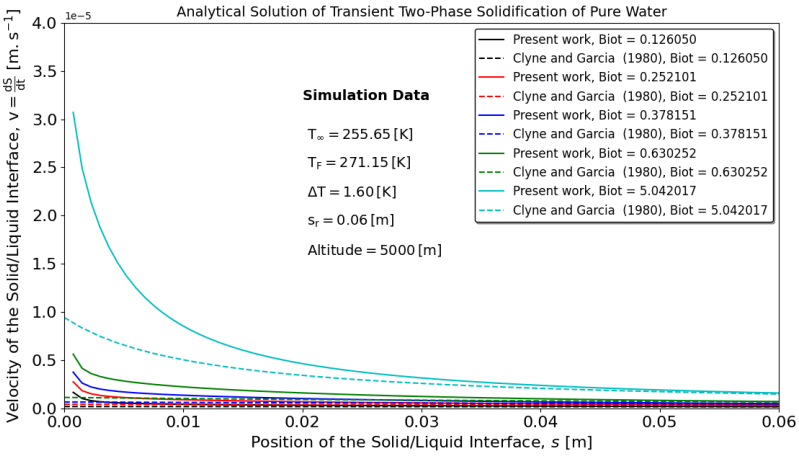

(A)

DOI: 10.3844/ajeassp.2026.88.116

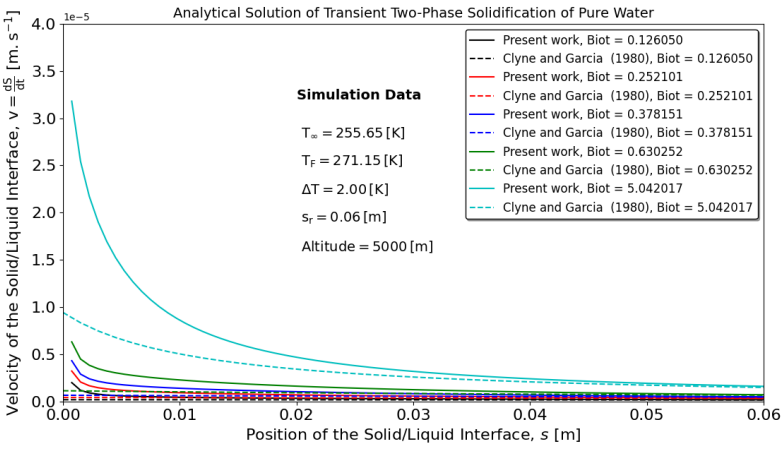

(B)

Fig. 9: Comparison of analytical solutions for one-dimensional water freezing under solid-liquid interface velocities, considering (A) 1.6 K and (B) 2.0 K superheat

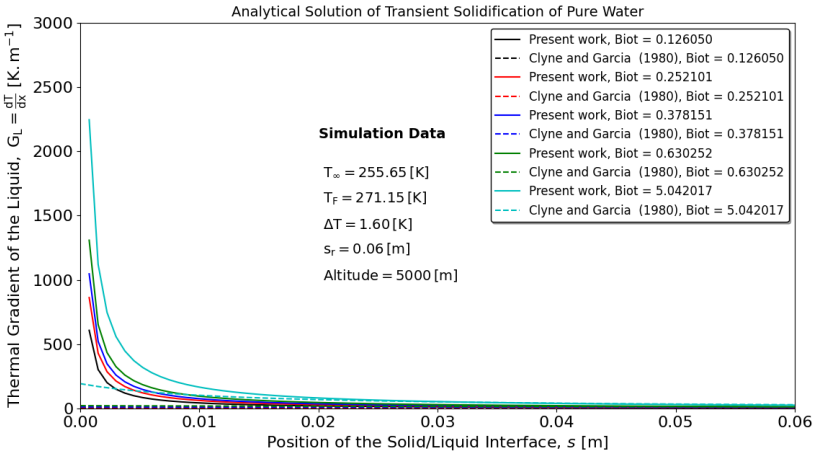

(B)

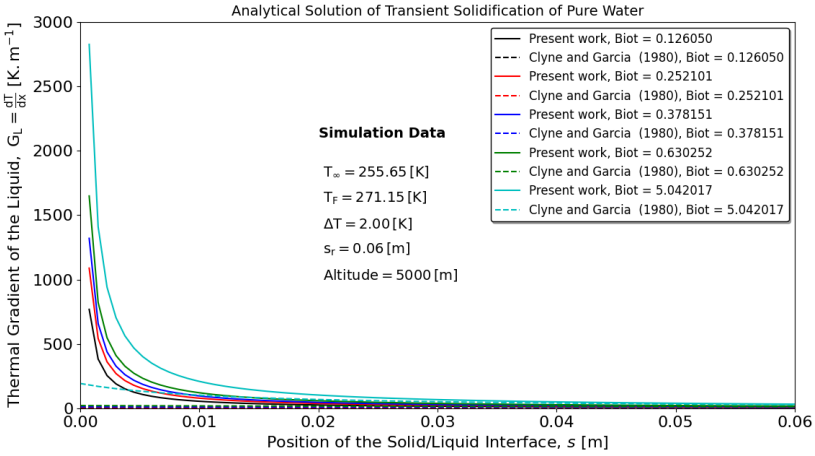

(B)

Fig. 10: Comparison of analytical solutions for one-dimensional water freezing under thermal gradients, considering (A) 1.6 K and (B) 2.0 K superheat

DOI: 10.3844/ajeassp.2026.88.116

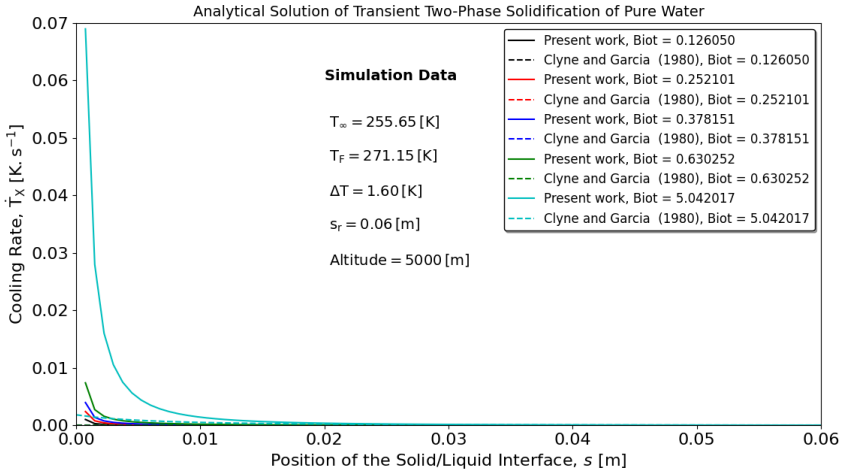

(A)

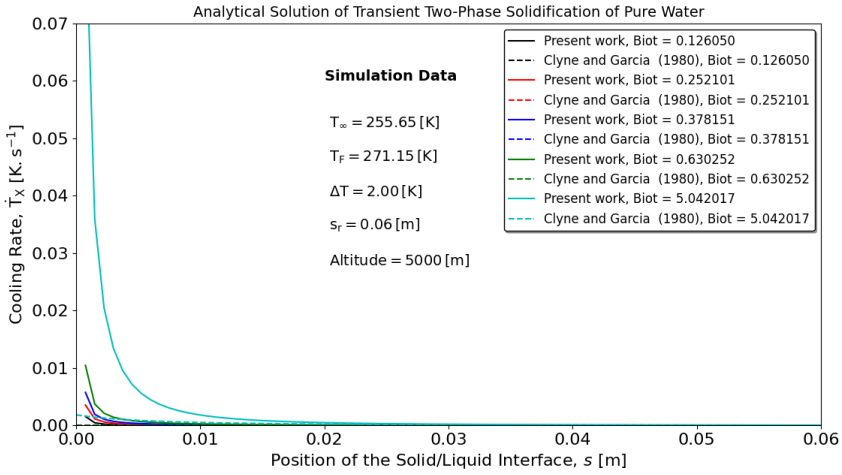

(B)

Fig. 11: Comparison of analytical solutions for one-dimensional water freezing under cooling rate, considering (A) 1.6 K and (B) 2.0 K superheat

An Important Solution for Melt Convection

An important solution, normally applied for horizontal transient solidification, is that of melt convection. In this case, the governing equations are the following:

$$\frac{\partial^2 T_S}{\partial x^2} = \frac{1}{\alpha_S}\frac{\partial T}{\partial t}\ 0 < x < s(t) \tag{66}$$

$$\frac{\partial^2 T_L}{\partial x^2} = \frac{1}{\alpha_l}\frac{\partial T}{\partial t}\ s(t) < x < +\infty \tag{67}$$

$$t = 0,\ 0 < x < +\infty,\ T = T_P \tag{68}$$

$$t > 0,\ x = 0,\ -k\frac{\partial T}{\partial x}\Big|_{x=0} = h(T - T_\infty) \tag{69}$$

$$t > 0,\ x = s(t),\ T = T_F \tag{70}$$

$$t > 0,\ x \to +\infty,\ T = T_P \tag{71}$$

$$\rho_S L \frac{ds}{dt} = k_S \frac{\partial T}{\partial x}\Big|_{x=^- s} - h_i(T_L(x =^- s, t) - T_F) \tag{72}$$

The temperature profile can now be expressed in terms of constant A_S and B_S:

$$\frac{T_S(x,t)-T_F}{T_\infty - T_F} = \frac{\left\{\operatorname{erfc}\left(\frac{x}{2\sqrt{\alpha_S t}}\right) - \exp\left(\frac{h\,x}{k_S} + \frac{h^2\alpha_S t}{k_S^2}\right)\operatorname{erfc}\left(\frac{x}{2\sqrt{a_S t}} + \frac{h\sqrt{\alpha_S t}}{k_S}\right) - \operatorname{erfc}(\varphi) + \exp\left(\frac{h\,s}{k_S} + \frac{h^2 s^2}{4\varphi^2 k_S^2}\right)\operatorname{erfc}\left(\varphi + \frac{h\,s}{2\varphi\,k_S}\right)\right\}}{\left\{1 - \operatorname{erfc}(\varphi) + \exp\left(\frac{h\,s}{k_S} + \frac{h^2 s^2}{4\varphi^2 k_S^2}\right)\operatorname{erfc}\left(\varphi + \frac{h\,s}{2\varphi\,k_S}\right)\right\}} \tag{73}$$

In a similar way, we can write:

$$\frac{T_S(x,t)-T_F}{T_\infty - T_F} = \frac{\left\{\operatorname{erfc}\left(\frac{x}{2\sqrt{\alpha_S t}}\right) - \exp\left(\frac{h\,x}{k_S} + \frac{h^2\alpha_S t}{k_S^2}\right)\operatorname{erfc}\left(\frac{x}{2\sqrt{\alpha_S t}} + \frac{h\sqrt{\alpha_S t}}{k_S}\right) + \zeta(s,t)\right\}}{\psi(s,t)} \tag{74a}$$

$$\frac{T_S(x,s)-T_F}{T_\infty - T_F} = \frac{\left\{\operatorname{erfc}\left(\varphi\frac{x}{s}\right) - \exp\left(\frac{h\,x}{k_S} + \frac{h^2 s^2}{4\varphi^2 k_S^2}\right)\operatorname{erfc}\left(\varphi\frac{x}{s} + \frac{h\,s}{2\varphi\,k_S}\right) + \zeta(s,\varphi)\right\}}{\psi(s,\varphi)} \tag{74b}$$

The thermal gradient $T_S(x,t)$ in the vicinity of boundary $x = ^- s$ is found by deriving the temperature profile with respect to x, which has the following form:

$$\frac{\partial T_S(s,t)}{\partial x}\Big|_{x=^- s} = \frac{(T_F - T_\infty)}{\psi(s,t)}\left\{\frac{h}{k_S}\exp\left(\frac{h\,s}{k_S} + \frac{h^2\alpha_S t}{k_S^2}\right)\exp\left(\varphi + \frac{h\sqrt{\alpha_S t}}{k_S}\right) + \frac{2\varphi}{\sqrt{\pi}\,s\exp(\varphi^2)} - \frac{2\varphi}{\sqrt{\pi}\,s\exp\left[\left(\varphi + \frac{h\sqrt{\alpha_S t}}{k_S}\right)^2\right]}\exp\left(\frac{h\,s}{k_S} + \frac{h^2\alpha_S t}{k_S^2}\right)\right\} \tag{75a}$$

$$\frac{\partial T_S(s,\varphi)}{\partial x}\Big|_{x=^- s} = \frac{(T_F - T_\infty)}{\psi(s,\varphi)}\left\{\frac{h}{k_S}\exp\left(\frac{h\,s}{k_S} + \frac{h^2\,s^2}{4\,\varphi^2\,k_S^2}\right)\exp\left(\varphi + \frac{h\,s}{2\varphi\,k_S}\right) + \frac{2\varphi}{\sqrt{\pi}\,s\exp(\varphi^2)} - \frac{2\varphi}{\sqrt{\pi}\,s\exp\left[\left(\varphi + \frac{h\,s}{2\varphi\,k_S}\right)^2\right]}\exp\left(\frac{h\,s}{k_S} + \frac{h^2\,s^2}{4\,\varphi^2\,k_S^2}\right)\right\} \tag{75b}$$

$$\frac{\partial T_S(s,\varphi)}{\partial x}\Big|_{x=^- s} = \frac{(T_F - T_\infty)}{\psi(s,\varphi)}\frac{2\varphi}{s}\left\{\frac{Biot_{Env}}{2\varphi}\exp\left(Biot_{Env} + \frac{Biot_{Env}^2}{4\,\varphi^2}\right)\exp\left(\varphi + \frac{Biot_{Env}}{2\varphi}\right) + \frac{1}{\sqrt{\pi}\,\exp(\varphi^2)} - \frac{1}{\sqrt{\pi}\,\exp\left[\left(\varphi + \frac{Biot_{Env}}{2\varphi}\right)^2\right]}\exp\left(Biot_{Env} + \frac{Biot_{Env}^2}{4\,\varphi^2}\right)\right\} \tag{75c}$$

The liquid phase profile and its gradient can be deduced as follows:

$$\frac{T_L(x,t)-T_P}{T_F - T_P} = \frac{1}{\psi(s,t)}\left\{\operatorname{erfc}\left(\frac{s+x}{2\sqrt{\alpha_L t}}\right) - \exp\left(\frac{h_i\,(s+x)}{k_L} + \frac{h^2\alpha_L t}{k_L^2}\right)\operatorname{erfc}\left(\frac{s+x}{2\sqrt{\alpha_L t}} + \frac{h_i\sqrt{\alpha_L t}}{k_L}\right)\right\} \tag{76a}$$

$$\frac{T_L(x,t)-T_P}{T_F - T_P} = \frac{1}{\psi(s,t)}\left\{\operatorname{erfc}\left(\frac{s+x}{2\sqrt{\alpha_L t}}\right) - \exp\left(\frac{h_i\,(s+x)}{k_L} + \frac{h^2\alpha_L t}{k_L^2}\right)\operatorname{erfc}\left(\frac{s+x}{2\sqrt{\alpha_L t}} + \frac{h_i\sqrt{\alpha_L t}}{k_L}\right)\right\} \tag{76b}$$

The thermal gradient $T_S(x,t)$in the vicinity of boundary $x = ^- s$is found by deriving the temperature profile with respect to *x*, which has the following form:

$$\frac{\partial T_L(s,t)}{\partial x}\Big|_{x=^+ s} = \frac{(T_F - T_P)}{\psi_L(s,t)}\left\{\frac{h_i}{k_L}\exp\left(\frac{h_i\,s}{k_L} + \frac{h_i^2\alpha_L t}{k_L^2}\right)\operatorname{erfc}\left(n\varphi + \frac{h_i\sqrt{\alpha_L t}}{k_L}\right) + \frac{2n\varphi}{\sqrt{\pi}\,s\exp(n^2\varphi^2)} - \frac{2n\varphi}{\sqrt{\pi}\,s\,\exp\left[\left(n\varphi + \frac{h_i\sqrt{\alpha_L t}}{k_L}\right)^2\right]}\exp\left(\frac{h_i\,s}{k_L} + \frac{h^2\alpha_L t}{k_L^2}\right)\right\} \tag{77a}$$

$$\frac{\partial T_L(s,\varphi)}{\partial x}\Big|_{x=^+ s} = \frac{(T_F - T_P)}{\psi_L(s,\varphi)}\left\{\frac{h_i}{k_L}\exp\left(\frac{h_i\,s}{k_L} + n^2\,\frac{h_i^2\,s^2}{4\,\varphi^2\,k_L^2}\right)\operatorname{erfc}\left(n\varphi + n\frac{h_i\,s}{2\varphi\,k_L}\right) + \frac{2n\varphi}{\sqrt{\pi}\,s\exp(n^2\varphi^2)} - \frac{2n\varphi}{\sqrt{\pi}\,s\exp\left[\left(n\varphi + n\frac{h_i\,s}{2\varphi\,k_L}\right)^2\right]}\exp\left(\frac{h_i\,s}{k_L} + n^2\,\frac{h_i^2\,s^2}{4\,\varphi^2\,k_L^2}\right)\right\} \tag{77b}$$

$$\left.\frac{\partial T_L(s,\varphi)}{\partial x}\right|_{x=^+s} = \frac{(T_F-T_P)}{\psi_L(s,\varphi)}\frac{2\varphi}{s}\left\{\frac{Biot_i}{2\varphi}\exp\left(Biot_i + n^2\frac{Biot_i^2}{4\,\varphi^2}\right)\operatorname{erfc}\left(n\varphi + n\frac{Biot_i}{2\varphi}\right) + \frac{n}{\sqrt{\pi}\,\exp(n^2\varphi^2)} - \frac{n}{\sqrt{\pi}\,\exp\left[\left(n\varphi+n\frac{Biot_i}{2\varphi}\right)^2\right]}\exp\left(Biot_i + n^2\frac{Biot_i^2}{4\,\varphi^2}\right)\right\} \quad (77c)$$

Substituting the thermal gradient of the solid phase $k_S\left.\frac{\partial T}{\partial x}\right|_{x=^-s}$ and temperature profile $T_L(x=^- s,t)$ derived in Eq. (72) into the moving boundary interface:

$$\rho_S L\left(\frac{ds}{dt}-\Omega\right) = k_S\left.\frac{\partial T}{\partial x}\right|_{x=^-s} - h_i(T_L(x=^- s,t)-T_F)$$

Provides:

$$\rho_S L\left(\frac{2\varphi^2\alpha_S}{s}-\Omega\right) = k_S\frac{(T_F-T_\infty)}{\psi(s,\varphi)}\left\{\frac{h}{k_S}\exp\left(\frac{h\,s}{k_S}+\frac{h^2\,s^2}{4\,\varphi^2\,k_S^2}\right)\operatorname{erfc}\left(\varphi+\frac{h\,s}{2\varphi\,k_S}\right)+\frac{2\varphi}{\sqrt{\pi}\,s\exp(\varphi^2)}-\frac{2\varphi}{\sqrt{\pi}\,s\exp\left[\left(\varphi+\frac{h\,s}{2\varphi\,k_S}\right)^2\right]}\exp\left(\frac{h\,s}{k_S}+\frac{h^2\,s^2}{4\,\varphi^2\,k_S^2}\right)\right\} - h_i(T_L(x=^- s,t)-T_F) \quad (78a)$$

Rearranging Eq. (47) and substituting Eq. (46):

$$\frac{L}{c_{PS}(T_F-T_\infty)}\left(\varphi-\frac{h}{k_S}\frac{s}{\varphi}\right) = \frac{1}{\psi(s,\varphi)}\left\{\frac{hs}{k_S 2\varphi}\exp\left(\frac{h\,s}{k_S}+\frac{h^2\,s^2}{4\,\varphi^2\,k_S^2}\right)\operatorname{erfc}\left(\varphi+\frac{h\,s}{2\varphi\,k_S}\right)+\frac{1}{\sqrt{\pi}\,\exp(\varphi^2)}-\frac{1}{\sqrt{\pi}\,\exp\left[\left(\varphi+\frac{h\,s}{2\varphi\,k_S}\right)^2\right]}\exp\left(\frac{h\,s}{k_S}+\frac{h^2\,s^2}{4\,\varphi^2\,k_S^2}\right)\right\} - \frac{k_L}{k_S(T_F-T_\infty)}\frac{h_i\,s}{k_L 2\varphi}(T_L(x=^- s,t)-T_F) \quad (78b)$$

$$\frac{1}{Ste}\left(\varphi-\frac{Biot_{Env}}{\varphi}\right) = \frac{1}{\psi(s,\varphi)}\left\{\frac{Biot_{Env}}{2\varphi}\exp\left(Biot_{Env}+\frac{Biot_{Env}^2}{4\,\varphi^2}\right)\operatorname{erfc}\left(\varphi+\frac{Biot_{Env}}{2\varphi}\right)+\frac{1}{\sqrt{\pi}\,\exp(\varphi^2)}-\frac{1}{\sqrt{\pi}\,\exp\left[\left(\varphi+\frac{Biot_{Env}}{2\varphi}\right)^2\right]}\exp\left(Biot_{Env}+\frac{Biot_{Env}^2}{4\,\varphi^2}\right)\right\} - \frac{1}{N}\frac{Biot_i}{2\varphi}\frac{(T_L(x=^- s,t)-T_F)}{(T_F-T_\infty)} \quad (78c)$$

$$\frac{1}{Ste}\left(\varphi-\frac{Biot_{Env}}{\varphi}\right) = \frac{1}{\psi(s,\varphi)}\left\{\frac{Biot_{Env}}{2\varphi}\exp\left(Biot_{Env}+\frac{Biot_{Env}^2}{4\,\varphi^2}\right)\operatorname{erfc}\left(\varphi+\frac{Biot_{Env}}{2\varphi}\right)+\frac{1}{\sqrt{\pi}\,\exp(\varphi^2)}-\frac{1}{\sqrt{\pi}\,\exp\left[\left(\varphi+\frac{Biot_{Env}}{2\varphi}\right)^2\right]}\exp\left(Biot_{Env}+\frac{Biot_{Env}^2}{4\,\varphi^2}\right)\right\} - \frac{1}{N}\frac{Biot_i}{2\varphi}\frac{(T_P-T_F)}{(T_F-T_\infty)}\left(\frac{2\varphi}{Biot_i\,\psi_L(s,\varphi)}f(Biot_i,\varphi)\right) \quad (78d)$$

Where, $f(Biot_i,\varphi)$ is given by the following derivation: For determining the temperature at the liquid region ^+s,

$$-k_L\left.\frac{\partial T}{\partial x}\right|_{x=^+s} = -h_i(T_L(x=^+ s,t)-T_F) \quad (79)$$

And, by expressing these equations in terms of dimensionless numbers, by writing, $N=\frac{k_S}{k_L}$, $Ste=\frac{C_P(T_F-T_\infty)}{L}$, $\Theta_0=\frac{(T_P-T_F)}{(T_F-T_\infty)}$, $Biot_{Env}=\frac{h\,s}{k_S}$, $Biot_i=\frac{h_i\,s}{k_L}$, and from Eq. (29f), $\Omega^*=\frac{Biot_{Env}}{\varphi\,Ste}$, which provides:

$$\frac{h_i s}{2\varphi}[T_L(x=^+ s,t)-T_F] = \frac{s}{2\varphi}k_L\left.\frac{\partial T}{\partial x}\right|_{x=^+s} = \frac{s}{2\varphi}k_L\frac{(T_P-T_F)}{\psi_L(s,\varphi)}\left\{\frac{h_i}{k_L}\exp\left(\frac{h_i\,s}{k_L}+n^2\frac{h_i^2\,s^2}{4\,\varphi^2\,k_L^2}\right)\operatorname{erfc}\left(n\varphi+n\frac{h_i\,s}{2\varphi\,k_L}\right)+\frac{2n\varphi}{\sqrt{\pi}\,s\exp(n^2\varphi^2)}-\frac{2n\varphi}{\sqrt{\pi}\,s\exp\left[\left(n\varphi+n\frac{h_i\,s}{2\varphi\,k_L}\right)^2\right]}\exp\left(\frac{h_i\,s}{k_L}+n^2\frac{h_i^2\,s^2}{4\,\varphi^2\,k_L^2}\right)\right\} \quad (80a)$$

$$\frac{h_i s}{k_L 2\varphi}[T_L(x =^{+} s,t) - T_F] = \frac{(T_P - T_F)}{\psi_L(s,\varphi)}\left\{\frac{h_i s}{2\varphi\, k_L} exp\left(\frac{h_i\, s}{k_L} + n^2\frac{h_i^2\, s^2}{4\,\varphi^2\, k_L^2}\right) erfc\left(n\varphi + n\frac{h_i\, s}{2\varphi\, k_L}\right) + \frac{n}{\sqrt{\pi}\ exp(n^2\varphi^2)} - \right.$$

$$\left.\frac{n}{\sqrt{\pi}\ exp\left[\left(n\varphi + n\frac{h_i\, s}{2\varphi\, k_L}\right)^2\right]} exp\left(\frac{h_i\, s}{k_L} + n^2\frac{h_i^2\, s^2}{4\,\varphi^2\, k_L^2}\right)\right\} \quad (80b)$$

Instead of this:

$$\frac{Biot_i}{2\varphi}[T_L(x =^{+} s,t) - T_F] = \frac{(T_P - T_F)}{\psi_L(s,\varphi)}\left\{\frac{Biot_i}{2\varphi}\exp\left(Biot_i + n^2\frac{Biot_i^2}{4\,\varphi^2}\right)\mathrm{erfc}\left(n\varphi + n\frac{Biot_i}{2\varphi}\right) + \frac{n}{\sqrt{\pi}\ \exp(n^2\varphi^2)} - \right.$$

$$\left.\frac{n}{\sqrt{\pi}\ \exp\left[\left(n\varphi + n\frac{h_i\, s}{2\varphi\, k_L}\right)^2\right]}\exp\left(Biot_i + n^2\frac{Biot_i^2}{4\,\varphi^2}\right)\right\} \quad (80c)$$

You must have this:

$$\frac{Biot_i}{2\varphi}[T_L(x =^{+} s,t) - T_F] = \frac{(T_P - T_F)}{\psi_L(s,\varphi)}\left\{\frac{Biot_i}{2\varphi}\exp\left(Biot_i + n^2\frac{Biot_i^2}{4\,\varphi^2}\right)\mathrm{erfc}\left(n\varphi + n\frac{Biot_i}{2\varphi}\right) + \frac{n}{\sqrt{\pi}\ \exp(n^2\varphi^2)} - \right.$$

$$\left.\frac{n}{\sqrt{\pi}\ \exp\left[\left(n\varphi + n\frac{Biot_i}{2\varphi}\right)^2\right]}\exp\left(Biot_i + n^2\frac{Biot_i^2}{4\,\varphi^2}\right)\right\} \quad (80c)$$

$$f(Biot_i,\varphi) = \left\{\frac{Biot_i}{2\varphi}\exp\left(Biot_i + n^2\frac{Biot_i^2}{4\,\varphi^2}\right)\mathrm{erfc}\left(n\varphi + n\frac{Biot_i}{2\varphi}\right) + \frac{n}{\sqrt{\pi}\ \exp(n^2\varphi^2)} - \frac{n}{\sqrt{\pi}\ \exp\left[\left(n\varphi + n\frac{Biot_i}{2\varphi}\right)^2\right]}\exp\left(Biot_i + n^2\frac{Biot_i^2}{4\,\varphi^2}\right)\right\} \quad (80d)$$

$$\frac{Biot_i}{2\varphi}[T_L(x =^{+} s,t) - T_F] = \frac{(T_P - T_F)}{\psi_L(s,\varphi)} f(Biot_i,\varphi) \quad (81)$$

Gives:

$$T_L(x =^{+} s,t) = T_F + \frac{2\varphi\,(T_P - T_F)}{Biot_i\,\psi_L(s,\varphi)} f(Biot_i,\varphi) \quad (82)$$

Substituting the thermal gradient of the solid phase $k_S \frac{\partial T}{\partial x}\Big|_{x=^{-}s}$ and temperature profile $T_L(x =^{-} s,t)$ derived in Eq. (80e) into the moving boundary interface:

$$\frac{1}{Ste}\left(\varphi - \frac{Biot_{Env}}{\varphi}\right) = \frac{1}{\psi(s,\varphi)}\left\{\frac{Biot_{Env}}{2\varphi}\exp\left(Biot_{Env} + \frac{Biot_{Env}^2}{4\,\varphi^2}\right)\mathrm{erfc}\left(\varphi + \frac{Biot_{Env}}{2\varphi}\right) + \frac{1}{\sqrt{\pi}\ \exp(\varphi^2)} - \frac{1}{\sqrt{\pi}\ \exp\left[\left(\varphi + \frac{Biot_{Env}}{2\varphi}\right)^2\right]}\exp\left(Biot_{Env} + \right.\right.$$

$$\left.\left.\frac{Biot_{Env}^2}{4\,\varphi^2}\right)\right\} - \frac{1}{N}\frac{(T_P - T_F)}{(T_F - T_\infty)}\left(\frac{1}{\psi_L(s,\varphi)}\left\{\frac{Biot_i}{2\varphi}\exp\left(Biot_i + n^2\frac{Biot_i^2}{4\,\varphi^2}\right)\mathrm{erfc}\left(n\varphi + n\frac{Biot_i}{2\varphi}\right) + \frac{n}{\sqrt{\pi}\ \exp(n^2\varphi^2)} - \frac{n}{\sqrt{\pi}\ \exp\left[\left(n\varphi + n\frac{Biot_i}{2\varphi}\right)^2\right]}\exp\left(Biot_i + \right.\right.\right.$$

$$\left.\left.\left. n^2\frac{Biot_i^2}{4\,\varphi^2}\right)\right\}\right) \quad (83)$$

An evaluation of the present solution could be the determination of liquid interface temperature for a set of interface and environment heat transfer coefficients, i.e., ., h_i and h, respectively. The thermophysical data can be found in Table 1.

The results for liquid domain solid-liquid interface temperature calculations are provided in Table 2. As can be observed, the interface temperature $T_L(x =^{-} s)$increases as the interface heat transfer coefficients $h_{i,j}$decrease.

Table 1: Thermophysical properties of pure Al

Property	Symbol	Unit	Value
Thermal condutivity of the solid	k_S	$W.m^{-1}K^{-1}$	213.0
Thermal condutivity of the liquid	k_L	$W.m^{-1}K^{-1}$	91.0
Specific heat of the solid	c_{PS}	$J.kg^{-1}K^{-1}$	1181.0
Specific heat of the liquid	c_{PL}	$J.kg^{-1}K^{-1}$	1086.0
Density of the solid	ρ_S	$kg.m^{-3}$	2550.0
Density of the liquid	ρ_L	$kg.m^{-3}$	2368.0
Thermal diffusivity of the solid	α_S	$m^2.s^{-1}$	7.073 x 10^{-5}
Thermal diffusivity of the liquid	α_l	$m^2.s^{-1}$	3.539 x 10^{-5}
Latent heat	L	$J.kg^{-1}$	397500.0
Parameter	n	-	1.41377
Parameter N	N	-	2.34066
Fusion temperature	T_F	K	933.15
Pouring temperature	T_P	K	970.48
Enviroment Temperature	T_∞	K	298.15
Environment heat transfer	h	$W.m^{-2}K^{-1}$	400
Interface heat transfer coefficient 1	$h_{i,1}$	$W.m^{-2}K^{-1}$	1800
Interface heat transfer coefficient 2	$h_{i,2}$	$W.m^{-2}K^{-1}$	1600
Interface heat transfer coefficient 3	$h_{i,3}$	$W.m^{-2}K^{-1}$	1400
Interface heat transfer coefficient 4	$h_{i,4}$	$W.m^{-2}K^{-1}$	800
Interface heat transfer coefficient 5	$h_{i,5}$	$W.m^{-2}K^{-1}$	500

Table 2: Calculation of liquid-domain temperature at the solid-liquid interface

Interface heat transfer coefficient, h_i	Temperature at $x =^- s,\ T_L(x =^- s, t)$
$h_{i,1}$	949.18K
$h_{i,2}$	950.74K
$h_{i,3}$	952.57K
$h_{i,4}$	960.31K
$h_{i,5}$	963.69K

Conclusion

- The results obtained with both the classical and the new transient solidification analytical solutions for the set of pure metals studied lead to the following conclusions
- Both models predict virtually identical interface velocities for all of the investigated materials
- The agreement seen for the velocity does not extend to the thermal gradient and the cooling rate values. The new model treats the Biot number rigorously, based on fundamental mathematical and physical principles that explicitly account for the convective nature of the problem; consequently, it yields steeper and more accurate gradients and cooling rates
- Classical literature solutions for the similarity variable usually assume a pure quadratic temperature profile and rely on a single function the error function erf(x) for the solid phase. In contrast, the present solution contains both a quadratic and a linear component in the similarity variable. The solid phase solution, therefore, employs the complementary error function erfc(x) and the exponential of the complementary error function, exp(x) erfc(x), which enables it to capture the steep gradients and high cooling rates observed experimentally
- The core formulation of the new model incorporates convective boundary conditions by using first and second order Biot numbers within the solidified layer. Adding convection to the classical solidification solution for a prescribed temperature, on the other hand, is essentially a mathematical artifice—a useful approximation that does not fully satisfy the convective boundary condition
- Overall, the new analytical framework provides a more physically consistent description of transient solidification under convective heat transfer than the classical approach

Declarations

Competing interests: The authors declare that they have no known competing financial interests or personal relationships that could have appeared to influence the work reported in this paper.

Acknowledgment

The authors acknowledge the financial support provided by CAPES (Coordenação de Aperfeiçoamento de Pessoal de Nível Superior Brasil Finance Code 001) and CNPq (National Council for Scientific and Technological Development). A.L.S. Moreira, from Federal University of Pará, is also acknowledged for reviewing the manuscript. Special thanks are extended to G.F.A. Santos for assistance with data preparation and curation.

Funding Information

The authors acknowledge the financial support provided by CAPES (Coordenação de Aperfeiçoamento de Pessoal de Nível Superior - Brazil), Finance Code 001 and Grant 88881.707312/2022-01, and CNPq (National Council for Scientific and Technological Development - Brazil) Grant 301502/2022-6.

Authors' Contributions

Gueber Elias Mendes Santos Júnior: Software formal analysis resources funding acquisition**.**
Fernando S. Rocha: Formal analysis.
Ana Beatriz S. Silva and Davi A. R. Carmo: Formal analysis writing original draft preparation.
Mateus O. Silva: Writing original draft preparation.
Ivaldo L Ferreira: Conceptualization methodology software investigation data curation writing review and edited visualization funding acquisition All authors have read and agreed to the published version of the manuscript.

Availability of Data and Materials

The data that support the findings of this study are available from the corresponding author upon reasonable request.

References

Akhtar, S., Xu, M., & Sasmito, A. P. (2021). Development and validation of a semi-analytical framework for droplet freezing with heterogeneous nucleation and non-linear interface kinetics. *International Journal of Heat and Mass Transfer*, *166*, 120734. https://doi.org/10.1016/j.ijheatmasstransfer.2020.120734

Alexandrov, D. V., Ivanov, A. A., & Alexandrova, I. V. (2018). Analytical solutions of mushy layer equations describing directional solidification in the presence of nucleation. *Philosophical Transactions of the Royal Society A: Mathematical, Physical and Engineering Sciences*, *376*(2113), 20170217. https://doi.org/10.1098/rsta.2017.0217

Alexandrov, D. V., Ivanov, A. A., & Alexandrova, I. V. (2018). Analytical solutions of mushy layer equations describing directional solidification in the presence of nucleation. *Philosophical Transactions of the Royal Society A: Mathematical, Physical and Engineering Sciences*, *376*(2113), 20170217. https://doi.org/10.1098/rsta.2017.0217

Alsulami, R. A., Zope, T. M., Premnath, K., & Aljaghtham, M. (2023). Convectively cooled solidification in phase change materials in different configurations subject to internal heat generation: Quasi-steady analysis. *Applied Thermal Engineering*, *221*, 119849. https://doi.org/10.1016/j.applthermaleng.2022.119849

Álvarez Hostos, J. C., Bencomo, A. D., Puchi Cabrera, E. S., & Figueroa Poleo, I. M. (2018). A pseudo-transient heat transfer simulation of a continuous casting process, employing the element-free Galerkin method. *International Journal of Cast Metals Research*, *31*(1), 47–55. https://doi.org/10.1080/13640461.2017.1366002

Carslaw, H. S., & Jaeger, J. C. (1959). *Conduction of heat in solids*.

Carvalho, I. S., Cotta, R. M., Naveira-Cotta, C. P., & Tiwari, M. K. (2021). Hybrid integral transform analysis of supercooled droplets solidification. *Proceedings of the Royal Society A: Mathematical, Physical and Engineering Sciences*, *477*(2248), 20200874. https://doi.org/10.1098/rspa.2020.0874

Cassia Lima Pimenta, de P. V., de Sousa Rocha, J. R., & Marcondes, F. (2022). Thermomechanical investigation of the continuous casting of ingots using the element-based Finite-Volume Method. *European Journal of Mechanics - A/Solids*, *96*, 104724. https://doi.org/10.1016/j.euromechsol.2022.104724

Clyne, T. W., & Garcia, A. (1980). Assessment of a new model for heat flow during unidirectional solidification of metals. *International Journal of Heat and Mass Transfer*, *23*(6), 773–782. https://doi.org/10.1016/0017-9310(80)90031-9

Crank, J. (1981). How to deal with moving boundaries in thermal problems. *Numerical Methods in Heat Transfer*, 177–200.

Crank, J. (1984). *Free and moving boundary problems*.

Davey, K. (1993). An analytical solution for the unidirectional solidification problem. *Applied Mathematical Modelling*, *17*(12), 658–663. https://doi.org/10.1016/0307-904x(93)90076-s

Ferreira, I. L., dos Santos, C. A., Garcia, A., & Voller, V. R. (2004). Analytical, numerical, and experimental analysis of inverse macrosegregation during upward unidirectional solidification of Al-Cu alloys. *Metallurgical and Materials Transactions B*, *35*(2), 285–297. https://doi.org/10.1007/s11663-004-0030-8

Fezi, K., & Krane, M. J. M. (2015). Uncertainty Quantification in Solidification Modelling. *IOP Conference Series: Materials Science and Engineering*, *84*, 012001. https://doi.org/10.1088/1757-899x/84/1/012001

Furzeland, R. M. (1977). *A survey of the formulation and solution of free and moving boundary (Stefan) problems*.

Furzeland, R. M. (1977). *A survey of the formulation and solution of free and moving boundary (Stefan) problems*.

Garcia, A., & Prates, M. (1978). Mathematical model for the unidirectional solidification of metals: I. cooled molds. *Metallurgical Transactions B*, *9*(3), 449–457. https://doi.org/10.1007/bf02654420

Garcia, A., Clyne, T. W., & Prates, M. (1979). Mathematical model for the unidirectional solidification of metals: II. Massive molds. *Metallurgical Transactions B*, *10*(1), 85–92. https://doi.org/10.1007/bf02653977

Garg, A., & Singhal, G. (2022). Mathematical modeling for transient thermal performance analysis of phase change material-based heat exchanger. *Applied Thermal Engineering*, *216*, 119029. https://doi.org/10.1016/j.applthermaleng.2022.119029

Govindasamy, D., & Kumar, A. (2023). Experimental analysis of solar panel efficiency improvement with composite phase change materials. *Renewable Energy*, *212*, 175–184. https://doi.org/10.1016/j.renene.2023.05.028

Hunziker, O. (2001). Theory of plane front and dendritic growth in multicomponent alloys. *Acta Materialia*, *49*(20), 4191–4203. https://doi.org/10.1016/s1359-6454(01)00313-5

Ivaldo Leão, F., Gueber Elias M., S. J., & Antonio Luciano Seabra, M. (2024). On the derivation of unsteady closed-form analytical solution for the solidification of pure and eutectic materials with boundary conditions of the third kind. *Research Square*. https://doi.org/10.21203/rs.3.rs-3906701/v1

Ivaldo Leão, Ferreira, Natália Cristina A., C., Gueber Elias M., S. J., Gonzaga, Fabrícia S., & Moreira, A. L. S. (2025). Computational analysis of transient solidification kinetics in aluminum-based multicomponent alloys for Graphical LHTES Modelling. *Journal Mater Engng*, *3*, 40–51.

Jost, W. (1952). *Diffusion in Solids, Liquids, Gases*. *201*. https://doi.org/10.1515/zpch-1952-2011-229

Li, C., Wen, J., Wang, L., Li, Y., & Lei, G. (2022). Modeling on transient microstructure evolution of solid-air solidification process under continuous cooling in liquid hydrogen. *International Journal of Hydrogen Energy*, *47*(81), 34640–34655. https://doi.org/10.1016/j.ijhydene.2022.08.027

Lipton, J., Garcia, A., & Heinemann, W. (1982). An analytical solution of directional solidification with mushy zone. *Archiv Für Das Eisenhüttenwesen*, *53*(12), 469–473. https://doi.org/10.1002/srin.198205182

Liu, Z.-A., Hou, J., Chen, Y., Liu, Z., Zhang, T., Zeng, Q., Dewancker, B. J., Meng, X., & Jiang, G. (2023). Effectiveness assessment of different kinds/configurations of phase-change materials (PCM) for improving the thermal performance of lightweight building walls in summer and winter. *Renewable Energy*, *202*, 721–735. https://doi.org/10.1016/j.renene.2022.12.009

Marques, L. P., Mesquita, S. Q., Maciel, A. C., Costa, R. B., França, R. S., Rocha, O. L., & Ferreira, I. L. (2025). Effect of Cooling Rate on the Secondary Dendritic Spacing of a Horizontally Solidified 6xxx Series Aluminum Alloy. *Materials Research*, *28*(suppl 1), e20250045. https://doi.org/10.1590/1980-5373-mr-2025-0045

Monde, A. D., & Chakraborty, P. R. (2017). 1-D diffusion based solidification model with volumetric expansion and shrinkage effect: A semi-analytical approach. *Physics Letters A*, *381*(39), 3349–3354. https://doi.org/10.1016/j.physleta.2017.08.033

Mori, A., & Akari, K. (1976). Methods of analysis of the moving boundary-surface problem. *International Chemical Engineering*, *16*(4), 734–744.

Pasupathy, A., Velraj, R., & Seeniraj, R. V. (2008). Phase change material-based building architecture for thermal management in residential and commercial establishments. *Renewable and Sustainable Energy Reviews*, *12*(1), 39–64. https://doi.org/10.1016/j.rser.2006.05.010

Quaresma, J. M. V., Santos, C. A., & Garcia, A. (2000). Correlation between unsteady-state solidification conditions, dendrite spacings, and mechanical properties of Al-Cu alloys. *Metallurgical and Materials Transactions A*, *31*(12), 3167–3178. https://doi.org/10.1007/s11661-000-0096-0

Rappaz, M., Jacot, A., & Boettinger, W. J. (2003). Last-stage solidification of alloys: Theoretical model of dendrite-arm and grain coalescence. *Metallurgical and Materials Transactions A*, *34*(3), 467–479. https://doi.org/10.1007/s11661-003-0083-3

Rocha, F. S., Costa, T. G., Oliveira, A. G., Costa, T. A., Ferreira, I. L., & Rocha, O. L. (2020). Transient heat flow parameters and microstructure of the upward solidified eutectic Al–Si alloy: a theoretical and experimental study. *Philosophical Magazine*, *100*(21), 2659–2676. https://doi.org/10.1080/14786435.2020.1785646

Saha, S. K., & Dutta, P. (2015). Performance Analysis of Heat Sinks with Phase-Change Materials Subjected to Transient and Cyclic Heating. *Heat Transfer Engineering*, *36*(16), 1349–1359. https://doi.org/10.1080/01457632.2015.1003714

Santos Júnior, G. E. M. (2024). Transient Solidification of Pure and Eutectic Metals: Exact solution for semi-infinite systems.

Swaminathan, C. R., & Voller, V. R. (1997). A generalized formulation of latent heat functions in enthalpy-based mathematical models for multicomponent alloy solidification systems. *Metallurgical and Materials Transactions B*, *40*(12), 143–145. https://doi.org/10.1007/s11663-006-0094-8

Tourret, D., & Karma, A. (2016). Three-dimensional dendritic needle network model for alloy solidification. *Acta Materialia*, *120*, 240–254. https://doi.org/10.1016/j.actamat.2016.08.041

Trojan, M. (2014). Transient Heat Conduction in Semi-infinite Solid with Surface Convection. *Encyclopedia of Thermal Stresses*, 6181–6186. https://doi.org/10.1007/978-94-007-2739-7_415

Voller, V. R. (2009). Analytical models of solidification phenomena. *Transactions of the Indian Institute of Metals*, *62*(4–5), 279–283.

Wang, J.-X., Qian, J., Wang, N., Zhang, H., Cao, X., Liu, F., & Hao, G. (2023). A scalable micro-encapsulated phase change material and liquid metal integrated composite for sustainable data center cooling. *Renewable Energy*, *213*, 75–85. https://doi.org/10.1016/j.renene.2023.05.106

Yang, L., Jin, X., Zhang, Y., & Du, K. (2021). Recent development on heat transfer and various applications of phase-change materials. *Journal of Cleaner Production*, *287*, 124432. https://doi.org/10.1016/j.jclepro.2020.124432

Zhou, C., & Wu, S. (2019). Medium- and high-temperature latent heat thermal energy storage: Material database, system review, and corrosivity assessment. *International Journal of Energy Research*, *43*(2), 621–661. https://doi.org/10.1002/er.4216